

# Inertial-like waves in rigidly-rotating odd viscous liquids

E.Kirkinis<sup>†</sup> and M. Olvera de la Cruz

Department of Materials Science & Engineering, Robert R. McCormick School of Engineering and Applied Science, Northwestern University, Evanston IL 60208 USA  
Center for Computation and Theory of Soft Materials, Northwestern University, Evanston IL 60208 USA

(Received xx; revised xx; accepted xx)

In a recent communication we showed that an odd viscous liquid in three spatial dimensions gives rise to Taylor columns, inertial waves and conservation of helicity. When an odd viscous liquid is subjected to rigid body rotation however, there is in addition a plethora of other phenomena that need to be clarified. In this paper we show that an incompressible three dimensional or compressible in two dimensions odd viscous liquid gives rise to both oscillatory and evanescent waves or a combination of the two. By evanescent we mean that along at least one of the spatial directions the velocity field, or an envelope thereof, increases or decreases exponentially. Thus, these latter waves can become prominent in the vicinity of a solid boundary. Helicity is conserved in such a flow composed of plane-polarized waves. The combination of rotation and odd viscosity gives rise to some unconventional behavior. In certain parameter regimes, plane polarized inertial waves may acquire a non-convex dispersion relation, known to become associated with oscillatory soliton tails and dispersive shocks in the presence of nonlinear terms. Maxima of the group velocity appear at angles  $\neq \frac{\pi}{2}$  between the axis of rotation and the wavevector. The corresponding direction of energy wave-packet propagation and helical particle paths can thus be chosen at will by a prudent election of odd viscosity and angular velocity parameter regimes. We show that recent numerical experiments on a two-dimensional compressible odd viscous liquid establishing the existence of topological waves near a boundary can be understood as evanescent inertial waves described by our formulation. The presence or absence of scattering of density waves in such a liquid is interpreted with respect to the motion of a disturbance with subsonic or supersonic speeds, respectively, the delineation of which is caused by odd viscosity coupled to rigid rotation-mediated renormalization of the speed of sound. This offers an explanation alternative to the one based on topological numbers. Another byproduct of this analysis is the agreement obtained between the theoretical predictions of a linear analysis and their nonlinear numerical counterparts.

**Key words:**

---

## 1. Introduction

Odd viscous liquids are dissipationless as they do not give rise to viscous heating (Landau & Lifshitz 1987; Kirkinis & Andreev 2019). They were introduced by Avron

<sup>†</sup> Email address for correspondence: kirkinis@northwestern.edu

(1998) following previous studies of the quantum Hall effect (Avron *et al.* 1995) and are endowed with a preferred direction determined, for instance, by a magnetic field (Lifshitz & Pitaevskii 1981, §13 & §58). Recent experiments on active liquids established the existence of the odd viscosity coefficient which acted to suppress surface undulations in a manner resembling surface tension. (Soni *et al.* 2019). Odd viscous liquids show dispersive behavior and a tendency to moderate singular behavior (Kirkinis *et al.* 2022).

A three-dimensional odd viscous liquid supports inertial-type waves because it is endowed with a restoring mechanism (Kirkinis & Olvera de la Cruz 2023) in the same sense that a fluid particle is restored back to its equilibrium position in a rigidly-rotating liquid (Batchelor 1967; Davidson 2013). In addition, a body moving slowly in a quiescent three-dimensional odd viscous liquid will be accompanied by a liquid cylindrical column parallel to the axis of anisotropy whose generators circumscribe the body (Kirkinis & Olvera de la Cruz 2023). If such a liquid is, however, subjected to rigid-body rotation with a constant angular velocity  $\Omega$ , a varied behavior in its dispersion and its flow pattern is observed. There are now parameter regimes where the resulting velocity field can become purely oscillatory, purely exponential or a combination thereof.

In this article we consider a three-dimensional odd viscous liquid rigidly rotating with constant angular velocity  $\Omega$  about the  $z$ -axis. We have also chosen the axis of anisotropy implied by the odd viscous liquid constitutive law to be along the same axis. We establish the presence of inertial-like waves and classify them with a single parameter  $\kappa$  that can be real, imaginary or complex, corresponding to the velocity field being oscillatory, exponential, or a combination of the two. The exponentially decaying fields, are called evanescent waves and may become prominent near a solid boundary. This behavior emerged in recent experiments of rigidly-rotating liquids by the radial oscillation of a cylinder (Nosan *et al.* 2021). Recent numerical experiments of the periodic excitation of the liquid's density in a cylindrical container in compressible two-dimensional odd viscous liquids (Souslov *et al.* 2019) likewise showed the existence of velocity fields decaying exponentially away from a boundary. Here we show that this latter behavior can be encompassed by our formulation and be understood as evanescent waves as long as we stay away from a solid boundary (since boundary-layer effects arise there, whose description would require account of the nonlinear terms in the Navier-Stokes equations). Yet, the predictions of our theory are robust. For example, the vorticity is proportional to the density as this was numerically observed in (Souslov *et al.* 2019, Fig. S2) for the nonlinear flow. Likewise, in regions of low dissipation, as the ones considered here, the velocity and the vorticity of the three dimensional odd viscous liquid are parallel. This tendency of the two fields to alignment, even when *nonlinear* terms of the Navier-Stokes equations are included, is expected from general grounds (Pelz *et al.* 1985).

When odd viscous liquids are subjected to rigid-body rotation, their dispersion relation may lose convexity leading to some unconventional consequences. These include the appearance of caustics (Lighthill 1978) and dispersive shocks (Lowman & Hofer 2013). These are reminiscent of Cherenkov radiation (Landau & Lifshitz 1960) arising from particle motion whose speed exceeds the one of plane waves in the medium (Kuznetsov & Dias 2011). A tangible consequence of this convexity loss in two dimensions is the presence of (evanescent) waves near a boundary that do not scatter off an obstacle. This is because the speed of sound in an odd rigidly-rotating medium is reduced, leads disturbances to propagate with supersonic speed and thus propagate downstream an obstacle without scattering.

Our presentation style is that of clarity rather than generality. Because of the presence of a large number of parameters we first state the simplest possible results whose generalization will come at a later stage. This paper is thus organized as follows. In

section 2 we demonstrate with a parameter diagram delineating the various states, the diversity of behavior the aforementioned system acquires in an axisymmetric cylindrical frame with harmonic waves propagating about the cylinder axis. Thus, the velocity fields are Bessel, modified Bessel or Kelvin-type functions associated with the eigenvalue of a linear differential operator which is thus real, imaginary or complex. In section 3 we employ some illustrative uncommon examples to display this behavior. These include a generalization to odd viscous liquids of a recent experimental study of evanescent waves in a rotating liquid (Nosan *et al.* 2021). As an outcome of this formulation we show that the vorticity and velocity fields are aligned even for exponentially-increasing/decreasing inertial waves. When the cylindrical geometry is abandoned and plane-polarized waves are considered, more restrictions come into place since the wavenumber is considered to be real. The plane polarized waves of an odd viscous liquid rotating rigidly make clear the presence of non-convex dispersion relation. Thus, caustics may arise as a consequence of propagating waves in rotating odd viscous liquids (Lighthill 1978; Ostrovsky & Potapov 1999). We briefly discuss parameter regimes where this behavior can take place. We study these effects in section 5. In section 5.1 we revisit the problems of the previous sections by including a second odd viscous stress tensor and thus a second odd viscosity coefficient we call  $\eta_4$  (borrowing this notation from (Lifshitz & Pitaevskii 1981, §58). Such a general liquid is endowed with all the aforementioned behaviors and we show that it conserves helicity.

It is known that in two-dimensional incompressible odd viscous liquids odd viscosity does not modify the velocity fields when the boundary conditions exclusively pertain velocities specified on solid boundaries (Ganeshan & Abanov 2017; Kirkinis 2023). This is not the case however when the odd viscous liquid is compressible. We show in section 6.1 that a rigidly-rotating odd viscous liquid in a two-dimensional axisymmetric geometry gives rise to inertial waves whose parameters follow the same flow classification as in the three-dimensional case we developed earlier in section 2. In some sense, the density of the compressible two-dimensional liquid plays the role of the axial velocity of its three dimensional incompressible counterpart. A number of illustrative examples demonstrate the salient features of these cases. These include recent numerical experiments of topological waves that propagate near the boundary of a disk (Souslov *et al.* 2019). We show that away from boundaries this problem can be considered a special case of our theoretical formulation and the waves are of evanescent inertial-wave type. We argue that the question of scattering of topological waves from an obstacle is determined by the renormalized by odd viscosity-angular velocity sound speed. Thus, disturbances propagating at supersonic speeds do not scatter off obstacles and the information of the presence of the obstacle exists only downstream (along a characteristic cone). On the other hand disturbances propagating at subsonic speeds will soon propagate everywhere in the container.

## 2. Inertial-like waves in a three dimensional rigidly-rotating incompressible odd viscous liquid

Consider an inviscid odd viscous liquid rotating rigidly about the  $\hat{z}$  axis with angular velocity  $\Omega$  (cf. Fig. 1). For an axially symmetric wave propagating along the axis the time and axial dependence are given by the factor  $\exp[i(kz - \omega t)]$  where the frequency  $\omega$  and wave number  $k$  along the axis are both real. We consider cylindrical polar coordinates  $r, \phi, z$ , and fields that are independent of  $\phi$ . We neglect the nonlinear terms by assuming small-amplitude motions. For completeness we display the form of the odd viscous stress in polar cylindrical coordinates (cf. Fig. 1) corresponding to one of the odd viscosity

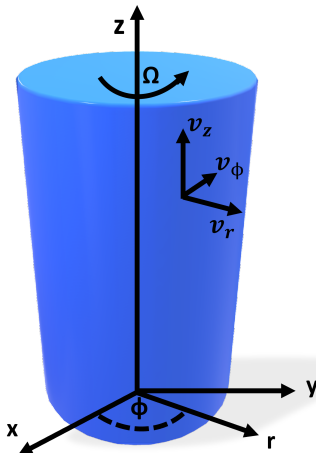


Figure 1: Three-dimensional odd viscous liquid rotating with angular velocity  $\Omega$  about the  $\hat{\mathbf{z}}$  axis. In cylindrical coordinates the velocity field is  $\mathbf{v} = v_r \hat{\mathbf{r}} + v_\phi \hat{\boldsymbol{\phi}} + v_z \hat{\mathbf{z}}$  in the frame of reference rotating with the liquid.

coefficients (we refer the reader to (Kirkinis & Olvera de la Cruz 2023) for the general form of the odd stress tensor):

$$\boldsymbol{\sigma}' = \eta_o \begin{pmatrix} -(\partial_r v_\phi - \frac{1}{r} v_\phi + \frac{1}{r} \partial_\phi v_r) & \partial_r v_r - \frac{1}{r} v_r - \frac{1}{r} \partial_\phi v_\phi & 0 \\ \partial_r v_r - \frac{1}{r} v_r - \frac{1}{r} \partial_\phi v_\phi & \partial_r v_\phi - \frac{1}{r} v_\phi + \frac{1}{r} \partial_\phi v_r & 0 \\ 0 & 0 & 0 \end{pmatrix}, \quad (2.1)$$

where  $\eta_o (> 0)$  is the coefficient of dynamic odd viscosity. Here the liquid is three-dimensional, and the velocity field satisfies the incompressibility condition

$$\partial_r(rv_r) + \partial_\phi v_\phi + r\partial_z v_z = 0. \quad (2.2)$$

The constitutive law (2.1) implies that an axis of anisotropy has, by some fortuitous mechanism, been established pointing in the  $\hat{\mathbf{z}}$  direction. The same will be true for the second constitutive law that we will later consider in section 5.1.

The Navier-Stokes equations take the form

$$-i\omega v_r - 2\Omega v_\phi = -\frac{1}{\rho} \frac{\partial p'}{\partial r} - \nu_o \left[ \frac{1}{r} \frac{\partial}{\partial r} \left( r \frac{\partial v_\phi}{\partial r} \right) - \frac{v_\phi}{r^2} \right], \quad (2.3)$$

$$-i\omega v_\phi + 2\Omega v_r = \nu_o \left[ \frac{1}{r} \frac{\partial}{\partial r} \left( r \frac{\partial v_r}{\partial r} \right) - \frac{v_r}{r^2} \right], \quad (2.4)$$

$$-i\omega v_z = -\frac{ik}{\rho} p', \quad (2.5)$$

where  $p'$  is the variable part of the pressure in the wave and  $\nu_o \equiv \eta_o/\rho$  is the coefficient of kinematic odd viscosity. The incompressibility condition (2.2) becomes

$$\frac{1}{r} \frac{\partial}{\partial r} (rv_r) + ikv_z = 0. \quad (2.6)$$

It is possible to simplify system (2.3)-(2.5). Combining Eq. (2.5) and (2.6) we obtain  $p'/\rho = \omega v_z/k = \frac{i\omega}{k^2} \frac{1}{r} \frac{\partial}{\partial r} (rv_r)$ . Employing the identity  $\frac{\partial}{\partial r} \left( \frac{1}{r} \frac{\partial}{\partial r} (rv_r) \right) = \frac{1}{r} \frac{\partial}{\partial r} \left( r \frac{\partial v_r}{\partial r} \right) - \frac{v_r}{r^2}$ , leads to an expression we will substitute into (2.3):  $\frac{1}{\rho} \frac{\partial p'}{\partial r} = \frac{i\omega}{k^2} \left[ \frac{1}{r} \frac{\partial}{\partial r} \left( r \frac{\partial v_r}{\partial r} \right) - \frac{v_r}{r^2} \right]$ .

The expressions  $\frac{1}{r} \frac{\partial}{\partial r} \left( r \frac{\partial}{\partial r} \right) - \frac{1}{r^2}$  appearing in the square brackets of (2.3) and (2.4) can

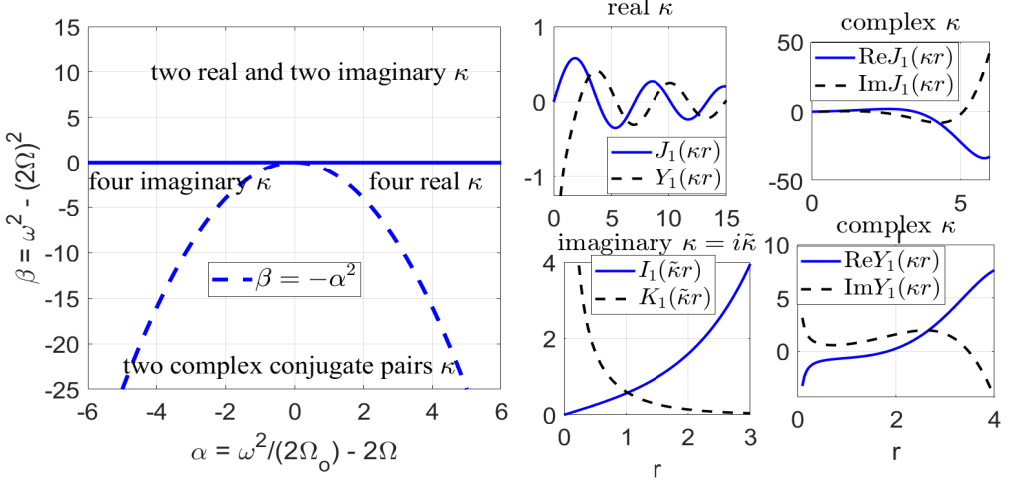


Figure 2: Left panel: Roots of Eq. (2.12) & (2.14) in the parameter space  $(\alpha, \beta)$  defined in Eq. (2.13). In the absence of rotation ( $\Omega = 0$ , so  $\beta > 0$ ) only the two real and two imaginary roots are possible as discussed in Kirkinis & Olvera de la Cruz (2023). Rich behavior exists in the presence of rotation. This includes the oscillatory Bessel functions for real  $\kappa$ , exponentially increasing/decreasing Bessel functions for  $\kappa$  imaginary and exponential-oscillating Bessel functions for complex  $\kappa$ . These behaviors are displayed in the right four panels.

be replaced by

$$\mathcal{L} = \partial_r^2 + \frac{1}{r}\partial_r - \frac{1}{r^2}. \quad (2.7)$$

Thus, the  $r$  and  $\phi$  momentum equations become

$$-i\omega v_r = -i\frac{\omega}{k^2}\mathcal{L}v_r - (\nu_o\mathcal{L} - 2\Omega)v_\phi, \quad (2.8)$$

$$-i\omega v_\phi = (\nu_o\mathcal{L} - 2\Omega)v_r. \quad (2.9)$$

Expressing the velocities  $v_r$  and  $v_\phi$  in terms of Bessel functions,  $v_r = AJ_1(\kappa r)$ ,  $v_\phi = BJ_1(\kappa r)$ , etc., (where  $A$  and  $B$  are constants to be determined by the boundary conditions and  $\kappa$  is an eigenvalue) the system (2.8) and (2.9) has a solution when the determinant of the coefficients of the resulting linear system

$$\frac{i(\nu_o\kappa^2 + 2\Omega)Bk^2 - A\kappa^2\omega}{k^2\omega} - A = 0, \quad -\frac{iA(\nu_o\kappa^2 + 2\Omega)}{\omega} - B = 0, \quad (2.10)$$

vanishes. This leads to a quartic equation for the determination of  $\kappa$

$$-\kappa^4 k^2 \nu_o^2 + (-4\Omega k^2 \nu_o + \omega^2) \kappa^2 - (2\Omega - \omega)(2\Omega + \omega) k^2 = 0, \quad (2.11)$$

with solutions

$$\kappa = \left[ \frac{-4\Omega k^2 \nu_o + \omega^2 \pm \sqrt{4k^4 \nu_o^2 \omega^2 - 8\Omega k^2 \nu_o \omega^2 + \omega^4}}{2\nu_o^2 k^2} \right]^{1/2}. \quad (2.12)$$

Here the frequency  $\omega$  and wave number  $k$  along the axis are both real quantities.  $\kappa$  can be real, imaginary or complex and it is this behavior of  $\kappa$  that gives rise to the diverse character of the velocity fields discussed in this paper.

---

$\alpha^2 + \beta$	$\alpha$	$\beta$	Type of root $\kappa$
+	+	+	two real, two imaginary
+	+	-	four real
+	-	-	four imaginary
-	-	-	two complex conjugate pairs

---

Table 1: Types of roots  $\kappa$  from Eq. (2.12)/(2.14)  $\nu_o \kappa^2 = \alpha \pm \sqrt{\alpha^2 + \beta}$  according to the sign of the parameters  $\alpha = \frac{\omega^2}{2\Omega_o} - 2\Omega$  and  $\beta = \omega^2 - (2\Omega)^2$  defined in Eq. (2.13)

---

To understand the structure of solutions we define an “odd” frequency and cumulative (frequency and frequency squared, respectively) parameters  $\alpha$  and  $\beta$  of the form

$$\Omega_o = \nu_o k^2, \quad \alpha = \frac{\omega^2}{2\Omega_o} - 2\Omega, \quad \beta = \omega^2 - (2\Omega)^2. \quad (2.13)$$

With this notation Eq. (2.12) becomes

$$\nu_o \kappa^2 = \frac{\omega^2}{2\Omega_o} - 2\Omega \pm \sqrt{\left(\frac{\omega^2}{2\Omega_o} - 2\Omega\right)^2 + \omega^2 - (2\Omega)^2} \equiv \alpha \pm \sqrt{\alpha^2 + \beta}. \quad (2.14)$$

Velocity fields obtained according to the type of  $\kappa$  are displayed in Fig. 2 and Table 1. Their functional form is

$$v_r = AJ_1(\kappa r)e^{i(kz - \omega t)}, \quad v_\phi = -iA \frac{\nu_o \kappa^2 + 2\Omega}{\omega} J_1(\kappa r)e^{i(kz - \omega t)}, \quad v_z = iA \frac{\kappa}{k} J_0(\kappa r)e^{i(kz - \omega t)}. \quad (2.15)$$

When the type of the eigenvalue  $\kappa$  has been decided upon, one can write down the dispersion relation

$$\omega = \pm \frac{k(\nu_o \kappa^2 + 2\Omega)}{\sqrt{k^2 + \kappa^2}} \quad (2.16)$$

which becomes nonconvex when  $\nu_o \Omega < 0$  and  $\kappa$  is real, and can thus be associated with unconventional behavior when nonlinear terms are included. A detailed discussion of this point is delegated to the polarized inertial wave section 5 and to its two-dimensional counterpart in section 7.2.

In Fig. 3 we display characteristic bifurcation curves showing how the real and imaginary parts  $\kappa_1$  and  $\kappa_2$ , respectively, of the parameter  $\kappa$  as solution of Eq. (2.12) change with real frequency  $\omega$ . On the left panel for values  $6 < \omega < 10 \equiv 2\Omega$  we see the four real values that form the “mexican hat”-type dispersion. It is clear that beyond these real  $\kappa$  values there are others that cannot be captured by a simple “plane-wave” analysis, such as the one we will develop below in section 5.

For a different set of parameter values the right panel of Fig. 3 shows either four imaginary  $\kappa$  values or two imaginary and two real. This behavior likewise cannot be captured by a plane-wave analysis. This situation is reminiscent of the discovery of Moffatt vortices (Moffatt 1964) who showed that empty spaces in a bifurcation diagram of parameters representing the flow near a corner, are populated by complex exponents of the streamfunction whose physical explanation was shown to be an infinite sequence of eddies.

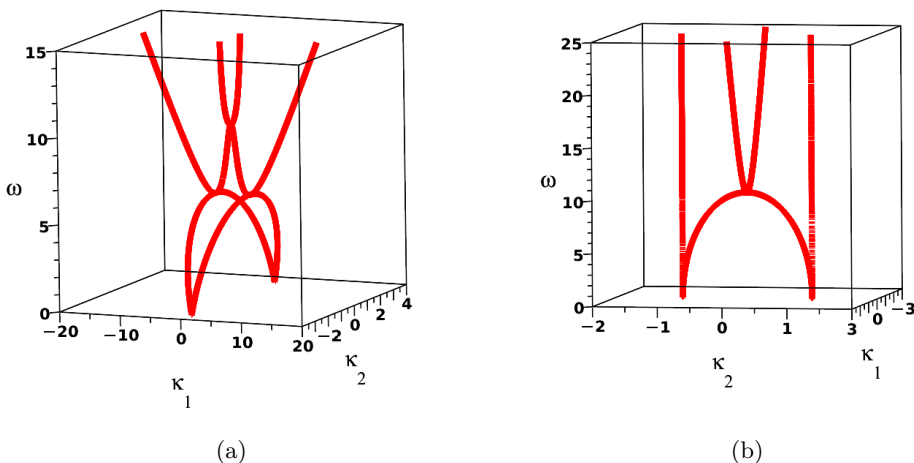


Figure 3: Real frequency  $\omega$  versus the real and imaginary parts of the eigenvalue  $\kappa = \kappa_1 + i\kappa_2$  derived as solution of Eq. (2.14). Left panel: Bifurcation diagram for the set of values  $(\Omega, \nu_o, k) = (5, 1, 1)$  (arbitrary units). This gives  $\alpha = \omega^2/2 - 10$ ,  $\beta = \omega^2 - 100$  and  $\alpha^2 + \beta = \omega^4/4 - 9\omega^2$ . There are two complex conjugate roots up to  $\omega = 6$ , where the radical in (2.14) changes sign. For  $6 < \omega < 10 = 2\Omega$  there are four real roots and beyond this, two imaginary and two real roots. Right panel: Bifurcation diagram for the set of values  $(\Omega, \nu_o, k) = (5, 10, 1)$  (arbitrary units). This gives  $\alpha = \omega^2/20 - 10$ ,  $\beta = \omega^2 - 100$  and  $\alpha^2 + \beta = \omega^4/400$ . There are four imaginary  $\kappa$  roots up to  $\omega = 10 = 2\Omega$ . Beyond this there are two imaginary and two real roots.

### 3. Illustrative examples

#### 3.1. Oscillating inertial waves

Consider the case where  $\omega \sim 2\Omega$  and thus  $\nu_o\kappa^2 \sim 2\alpha = 4\Omega \left( \frac{\Omega}{\Omega_o} - 1 \right)$  or  $\nu_o\kappa^2 = 0$  from Eq. (2.14). Two real roots exist as long as  $\Omega > \Omega_o \equiv \nu_o k^2$  and the velocity field is given by (2.15). This motion comprises regions between concentric cylinders of radius  $r_n$  such that

$$r_n \kappa = \gamma_n \quad (3.1)$$

and  $\gamma_n$  are the zeros of  $J_1(x)$ . Both  $v_r$  and  $v_\phi$  vanish at these cocentric circles and the fluid does not cross them. This case resembles one in (Kirkinis & Olvera de la Cruz 2023) and we only include the final results. We consider a liquid enclosed in a cylinder of radius  $r = b$ . This boundary will be a streamline located at an integral number of cells in the radial direction. Writing down the streamfunction

$$\psi(r, z) = \frac{\kappa}{3.83} r J_1(\kappa r) \sin(kz), \quad v_z = \frac{1}{r} \frac{\partial \psi}{\partial r}, \quad v_r = -\frac{1}{r} \frac{\partial \psi}{\partial z}, \quad (3.2)$$

we display the instantaneous streamlines in Fig. 4 where we chose  $\kappa b = \gamma_2 \sim 7.0156$ , the latter being the second zero of  $J_1(x)$ . Here the amplitude is modulated by the first zero of the Bessel function  $J_1(x)$  in a manner analogous to the rigidly-rotating case of a (non-odd) viscous liquid Fig. 7.6.4 of (Batchelor 1967, p.561).

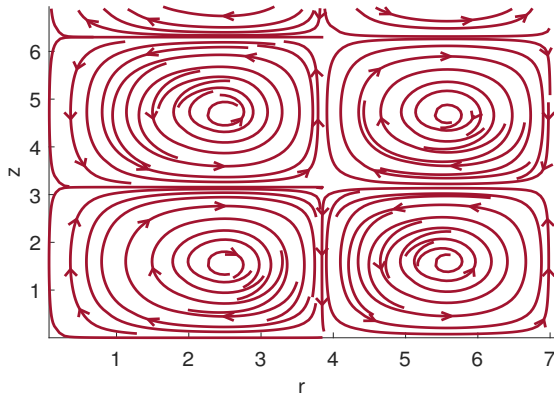


Figure 4: Instantaneous streamlines in the  $r - z$  plane with streamfunction (3.2), representing a simple harmonic wave propagating in the  $z$ - direction with phase velocity  $c_p = \omega/k$ . The line  $r = 0$  is the central axis of the cylinder and the line  $r = 7.0156 (= b)$  is the surface of the enclosing cylinder where the radial velocity  $v_r$  vanishes (we've chosen  $\kappa = 1$ ).

### 3.2. Evanescent inertial waves

Consider an annular cylinder of inner and outer radii  $R_1$  and  $R_2$  respectively where the inner boundary is being radially displaced harmonically with frequency  $\omega$ . The liquid is rotating as a whole with angular velocity  $\Omega$  about the central axis. This then is a system with the geometry employed in the recent experiments of (Nosan *et al.* 2021) which showed that a (not odd) rigidly-rotating three-dimensional incompressible liquid gives rise to evanescent waves at the cross-over frequency  $\omega \rightarrow 2\Omega$ . Assuming  $\omega = 2\Omega$  ( $\beta = 0$ ), we obtain two imaginary roots  $\kappa = \pm i\tilde{\kappa}$ , for real  $\tilde{\kappa}$  from (2.12) if  $0 < \Omega < \Omega_o (\equiv \nu_o k^2)$  and the solution reads

$$v_r = AI_1(\tilde{\kappa}r) + BK_1(\tilde{\kappa}r), \quad (3.3)$$

where by  $\tilde{\kappa}$  in this section only we denote the imaginary part of the roots of (2.14). Thus,

$$\tilde{\kappa} = 2\sqrt{\frac{\Omega}{\nu_o} \left(1 - \frac{\Omega}{\Omega_o}\right)}, \quad \Omega_o = \nu_o k^2 > \Omega. \quad (3.4)$$

Let

$$\eta(z, t) = \hat{\eta}e^{i(kz - \omega t)} \quad (3.5)$$

be the *radial* displacement of the inner boundary at  $r = R_1$  with complex  $\hat{\eta}$  which will excite inertial waves of oscillatory or evanescent character. Thus, the radial velocity satisfies

$$v_r(R_1, z, t) = \partial_t \eta = -i\omega\eta, \quad v_r(R_2, z, t) = 0. \quad (3.6)$$

The former is the leading order expression in the expansion of  $v_r(R_1 + \text{Re}\eta, z, t)$  in powers of the displacement  $\eta$ .

The boundary conditions (3.6) lead to the requirements  $v_r(R_1) = AI_1(\tilde{\kappa}R_1) + BK_1(\tilde{\kappa}R_1) = -i\omega\hat{\eta}$  and  $v_r(R_2) = AI_1(\tilde{\kappa}R_2) + BK_1(\tilde{\kappa}R_2) = 0$  from which we obtain

$$A = -i\omega\hat{\eta}K_1(\tilde{\kappa}R_2)J^{-1}, \quad B = -A\frac{I_1(\tilde{\kappa}R_2)}{K_1(\tilde{\kappa}R_2)}, \quad J = \begin{vmatrix} I_1(\tilde{\kappa}R_1) & I_1(\tilde{\kappa}R_2) \\ K_1(\tilde{\kappa}R_1) & K_1(\tilde{\kappa}R_2) \end{vmatrix}. \quad (3.7)$$

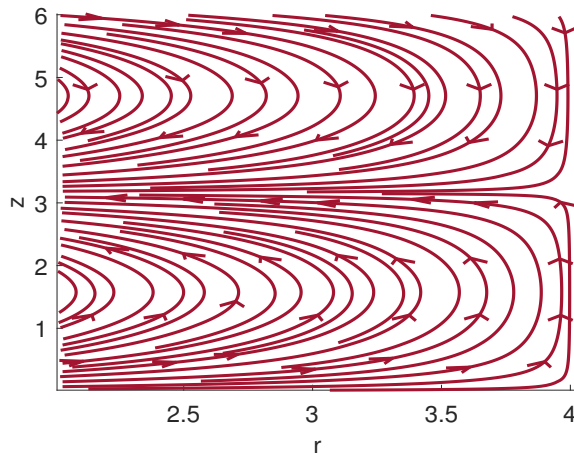


Figure 5: Instantaneous streamlines in the  $r - z$  plane of the velocity field (3.9) - (3.11), representing a forced harmonic wave propagating in the  $z$ - direction according to (3.5). The liquid is confined between the forced inner cylinder at  $r = R_1 = 2 + \text{Re}\hat{\eta}$  and the immobile external cylinder at  $r = R_2 = 4$ .

The solution simplifies somewhat if we cast  $A$  in polar form  $A = ae^{i\theta}$  for real  $a, \theta$ . Then,

$$a = \omega|\hat{\eta}|K_1(\tilde{\kappa}R_2)J^{-1}, \quad \theta = -\arctan \frac{\text{Re}\hat{\eta}}{\text{Im}\hat{\eta}}, \quad (3.8)$$

where  $|\hat{\eta}| = \sqrt{(\text{Re}\hat{\eta})^2 + (\text{Im}\hat{\eta})^2}$  and  $\text{Re}\hat{\eta}$  and  $\text{Im}\hat{\eta}$  are the real and imaginary parts of the complex number  $\hat{\eta}$ . We thus obtain,

$$v_r = \omega|\hat{\eta}|J^{-1} [I_1(\tilde{\kappa}r)K_1(\tilde{\kappa}R_2) - I_1(\tilde{\kappa}R_2)K_1(\tilde{\kappa}r)] \cos(kz - \omega t + \theta), \quad (3.9)$$

$$v_\phi = (2\Omega - \nu_o\tilde{\kappa}^2)|\hat{\eta}|J^{-1} [I_1(\tilde{\kappa}r)K_1(\tilde{\kappa}R_2) - I_1(\tilde{\kappa}R_2)K_1(\tilde{\kappa}r)] \sin(kz - \omega t + \theta), \quad (3.10)$$

$$v_z = -\omega|\hat{\eta}|J^{-1} \frac{\tilde{\kappa}}{k} [I_0(\tilde{\kappa}r)K_1(\tilde{\kappa}R_2) + I_1(\tilde{\kappa}R_2)K_0(\tilde{\kappa}r)] \sin(kz - \omega t + \theta). \quad (3.11)$$

Note the positive sign of  $K_0(\tilde{\kappa}r)$  in (3.11) obtained because  $K_n$  satisfies different derivative relations to  $I_n$ .

The solution (3.9)-(3.11) for evanescent waves in an odd viscous liquid is formally analogous to the one obtained by Nosan *et al.* (2021). Here however we solve a fourth order system and thus, in general, we obtain four  $\kappa$ 's. We display the streamlines in an  $r - z$  slice of the cylinder in Fig. 5.

#### 4. Helicity in axisymmetric, rigidly rotating odd viscous liquids

When the roots  $\kappa$  of Eq. (2.12) are real, one can easily show that the the vorticity of axisymmetric waves developed in section 2 is proportional to the velocity of the liquid. This generalizes the case of odd viscous liquid without rotation developed in (Kirkinis & Olvera de la Cruz 2023) and the results obtained here are identical to the non-rotating case

$$\text{curl}\mathbf{v} = \mp\sqrt{k^2 + \kappa^2}\mathbf{v}, \quad \text{and} \quad \mathbf{v} \cdot \text{curl}\mathbf{v} = \mp\sqrt{k^2 + \kappa^2}|\mathbf{v}|^2, \quad (4.1)$$

with the understanding that the frequency  $\omega$  in the present case satisfies the relation

$$\omega = \frac{(\nu_o\kappa^2 + 2\Omega)k}{\sqrt{k^2 + \kappa^2}}.$$

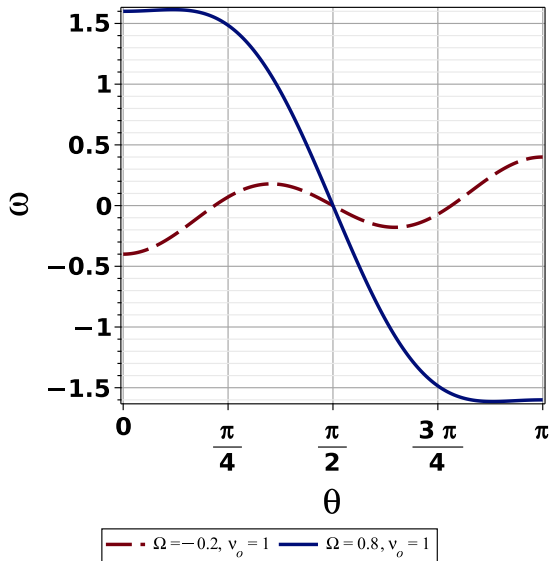


Figure 6: Plane-polarized wave dispersion  $\omega$  (Eq. (5.4)) versus angle  $\theta$  between the wavevector  $\mathbf{k}$  and the  $z$ - (anisotropy/rotation) axis (setting  $k = \nu_o = 1$ ). Of interest is the dashed curve denoting the existence of non-convex dispersion for the displayed parameters. At its inflection points the group velocity becomes maximum (cf. Fig. 7) and the second derivative  $|\partial_{k_i k_j}^2 \omega|$  vanishes (cf. Fig. 8), implying the presence of caustics and a breakdown of the longtime asymptotics.

We now show that vorticity is parallel to the velocity when  $\kappa$  is imaginary (the case of evanescent waves). From Eq. (2.15) with  $\kappa = i\tilde{\kappa}$  imaginary and  $\tilde{\kappa}$  real, we find that the vorticity

$$\text{curl} \mathbf{v} = k \frac{\nu_o \tilde{\kappa}^2 - 2\Omega}{\omega} v_r \hat{\mathbf{r}} + \frac{\omega}{\nu_o \tilde{\kappa}^2 - 2\Omega} \frac{k^2 - \tilde{\kappa}^2}{k} v_\phi \hat{\boldsymbol{\phi}} + k \frac{\nu_o \tilde{\kappa}^2 - 2\Omega}{\omega} v_z \hat{\mathbf{z}}. \quad (4.2)$$

The coefficients multiplying the velocities in (4.2) are equal to each other if

$$\omega^2 = \frac{k^2 (\nu_o \tilde{\kappa}^2 - 2\Omega)^2}{k^2 - \tilde{\kappa}^2} \quad (4.3)$$

and this is exactly the relation we obtain from (2.12) by solving for  $\omega^2$  when  $\kappa$  is imaginary. Eq. (4.3) introduces a constraint on the wavenumbers, that is,  $k^2 > \tilde{\kappa}^2$  for the frequency to remain real. Thus, overall we can write that

$$\text{curl} \mathbf{v} = \mp \sqrt{k^2 - \tilde{\kappa}^2} \mathbf{v}, \quad k > \tilde{\kappa}. \quad (4.4)$$

replacing  $\text{curl} \mathbf{v} = \mp \sqrt{k^2 + \kappa^2} \mathbf{v}$  that holds when  $\kappa$  as a root of (2.12) is real.

## 5. Plane-polarized waves induced in a rigidly-rotating liquid by odd viscosity

Plane-polarized waves in rigidly-rotating liquids support inertial waves (Landau & Lifshitz 1987, §14) and (Davidson 2013). In a previous communication we showed that plane polarized waves are also supported in a (non-rotating) odd viscous liquid (Kirkinis & Olvera de la Cruz 2023). It turns out that inertial waves that arise when rotation and

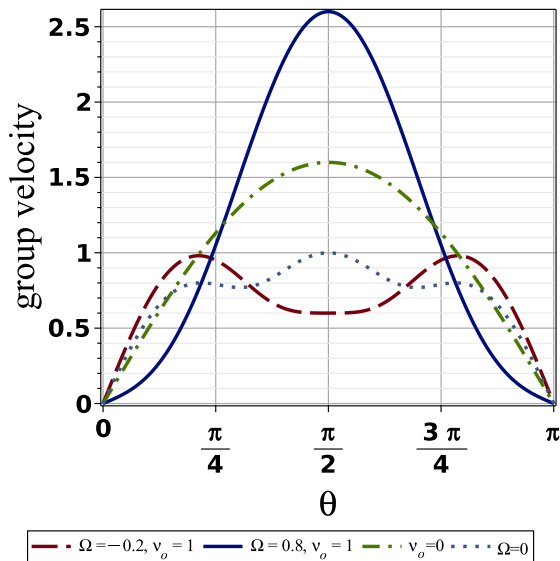


Figure 7: Plane-polarized wave group velocity (5.11) versus angle  $\theta$  between the wavevector  $\mathbf{k}$  and the  $z$ - (anisotropy) axis, setting  $k = \nu_o = 1$ . Of interest is the dashed curve denoting the existence of non-convex dispersion for the displayed parameters since the group velocity becomes maximum and the second derivative  $|\partial_{k_i k_j}^2 \omega|$  vanishes (cf. Fig. 8), implying the presence of caustics and a breakdown of the longtime asymptotics. The behavior denoted by the dashed line has implications on the helicity of the flow, since the maximum group velocity is found at a polar angle  $\theta$  not equal to  $\pi/2$  (which is the angle of maximum group velocity for a rigidly-rotating (not odd) liquid, cf. (Davidson 2013)).

odd viscosity are combined, present some special characteristics. For instance, below we show that the group velocity develops extrema where the propagation wavevector  $\mathbf{k}$  is *not* perpendicular to the rotation/anisotropy axis. This takes place when the dispersion  $\omega$  has an inflection point, which coincides with the vanishing of the determinant of the matrix  $\partial^2 \omega / \partial k_i \partial k_j$ . This implies that in such problems we are dealing with a non-convex dispersion relation. Nonconvex dispersions have been associated with the appearance of caustics leading to self-focusing of nonlinear waves. It is thus of some interest to classify the locations at which such behavior may arise.

The linearized vorticity equation of an odd viscous liquid subject to the constitutive law (2.1) obtains the form

$$\partial_t \text{curl} \mathbf{v} = (2\Omega - \nu_o \nabla_2^2) \frac{\partial \mathbf{v}}{\partial z}, \quad (5.1)$$

where  $\nabla_2^2 = \partial_x^2 + \partial_y^2$ . We seek plane-wave solutions of the form

$$\mathbf{v} = \mathbf{A} e^{i(\mathbf{k} \cdot \mathbf{r} - \omega t)}, \quad (5.2)$$

which leads to the requirement that  $\mathbf{A} \cdot \mathbf{k} = 0$  from the incompressibility condition.

Substituting the plane-wave solution into (5.1) we obtain

$$\omega \mathbf{k} \times \mathbf{v} = i [2\Omega + \nu_o (k_x^2 + k_y^2)] k_z \mathbf{v}. \quad (5.3)$$

From this equation and its counterpart obtained by taking the cross product of both sides

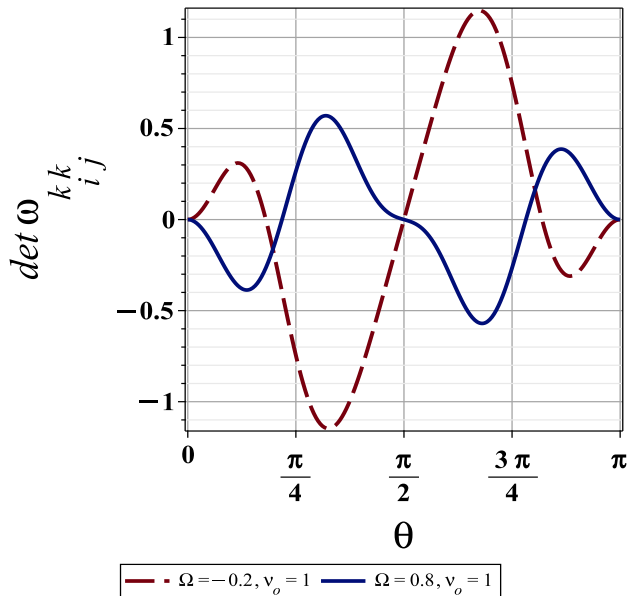


Figure 8: Determinant of the matrix  $\partial_{k_i k_j}^2 \omega$  in (5.12) versus angle  $\theta$  between the wavevector  $\mathbf{k}$  and the  $z$ - (anisotropy) axis, setting  $k = \nu_o = 1$ . Of interest is the dashed curve for the indicating parameter values, which, for the negative values of  $\Omega$  vanishes at angle  $\theta = \cos^{-1} \sqrt{\frac{F}{5\nu_o k^2}}$  (cf. second line of Table 2) corresponding to the inflexion points of the dispersion relation (cf. Fig. 6) and the extrema of the group velocity (cf. Fig. 7), indicating the presence of caustics (overlapping of space-time rays (Ostrovsky & Potapov 1999, Fig. 6.3)). The vanishing of the positive  $\Omega$  curve at  $\theta = \cos^{-1} \sqrt{\frac{2\Omega - k^2 \nu_o}{\nu_o k^2}}$  (cf. first line of Table 2) does not correspond to maxima of the group velocity.

with  $\mathbf{k}$  we obtain the dispersion relation (to avoid repetitiveness we skip the derivation details which can be found in (Kirkinis & Olvera de la Cruz 2023))

$$\omega = \pm \frac{[2\Omega + \nu_o(k_x^2 + k_y^2)] k_z}{k}, \quad \text{or} \quad \omega = \pm [2\Omega + \nu_o k^2 \sin^2 \theta] \cos \theta \quad (5.4)$$

where  $k = \sqrt{k_x^2 + k_y^2 + k_z^2}$  and in the latter equation  $\theta$  is the angle between the  $\mathbf{k}$  and the anisotropy/rotation  $z$ -axis. In Fig. 6 we plot the dispersion  $\omega$  (Eq. (5.4)) versus angle  $\theta$ . From the second of Eq. (5.4) it is clear that the dispersion not only vanishes at  $\theta = \pi/2$  as the case was for an inviscid fluid rotating with angular velocity  $\Omega$ , but also vanishes when

$$\theta = \cos^{-1} \frac{\sqrt{\nu_o(k^2 \nu_o + 2\Omega)}}{k \nu_o}, \quad (5.5)$$

for suitable values of the parameters, as is apparent in Fig. 6 (dashed line).

With the unit vector  $\hat{\mathbf{k}} = \frac{\mathbf{k}}{k}$  in the direction of the wave-vector and the complex amplitude  $\mathbf{A} = \mathbf{a} + i\mathbf{b}$  where  $\mathbf{a}$  and  $\mathbf{b}$  are real vectors, Eq. (5.3) and the dispersion relation (5.4) lead to  $\hat{\mathbf{k}} \times \mathbf{b} = \mathbf{a}$ , that is, the two vectors  $\mathbf{a}$  and  $\mathbf{b}$  are perpendicular to each other, are of the same magnitude and lie in the plane whose normal is  $\mathbf{k}$ . Thus, the

---

$\theta$ : root of Eq. (5.12)	group velocity $\mathbf{c}_g$ evaluated at a root $\theta$ of Eq. (5.12)
$\cos^{-1} \sqrt{\frac{2\Omega - k^2 \nu_o}{\nu_o k^2}}$	$\frac{4(k^2 \nu_o - \Omega)}{k} \hat{\mathbf{z}}$
$\cos^{-1} \sqrt{\frac{F}{5\nu_o k^2}}$	$\frac{\sqrt{F(5\nu_o k^2 - F)(5\nu_o k^2 + F - 10\Omega)}}{25\nu_o k^3} (\cos \phi \hat{\mathbf{x}} + \sin \phi \hat{\mathbf{y}}) + \frac{(F - 5\nu_o k^2 - 10\Omega)(F - 5\nu_o k^2)}{25\nu_o k^3} \hat{\mathbf{z}}$
$\frac{\pi}{2}$	$\frac{k^2 \nu_o + 2\Omega}{k} \hat{\mathbf{z}}$

---

Table 2: Summary of functional expressions attained by group velocity at its extrema determined by the roots of Eq. (5.12). The group velocity thus has extrema that differ from the known cases of zero rotation or zero odd viscosity, displayed in the third line. The roots displayed in the first column and the corresponding group velocities exist for different combinations of  $\Omega$  and  $\nu_o$  and the latter are displayed in Fig. 20.  $F = 2k^2 \nu_o + \sqrt{9k^4 \nu_o^2 + 12\Omega k^2 \nu_o + 84\Omega^2} + 8\Omega > 0$  and  $k = \sqrt{k_x^2 + k_y^2 + k_z^2}$ .

---

velocity field is circularly polarized in the plane defined by  $\mathbf{a}$  and  $\mathbf{b}$  and is of the form

$$\mathbf{v} = \mathbf{a} \cos(\mathbf{k} \cdot \mathbf{r} - \omega t) - \mathbf{b} \sin(\mathbf{k} \cdot \mathbf{r} - \omega t), \quad \mathbf{a} \perp \mathbf{b}. \quad (5.6)$$

Employing the negative sign of the dispersion relation (5.4), the above analysis leads to the same velocity field (5.6) but with the sense of the vectors  $\mathbf{a}$  and  $\mathbf{b}$  reversed:  $\hat{\mathbf{k}} \times \mathbf{b} = -\mathbf{a}$ .

It is of interest to calculate the direction of propagation of energy. We obtain

$$\left( \frac{\partial \omega}{\partial k_x}, \frac{\partial \omega}{\partial k_y} \right) = \frac{k_z [\nu_o (k^2 + k_z^2) - 2\Omega]}{k^3} (k_x, k_y), \quad \frac{\partial \omega}{\partial k_z} = \frac{[2\Omega + \nu_o (k_x^2 + k_y^2)] (k_x^2 + k_y^2)}{k^3}, \quad (5.7)$$

or, taking the  $z$  axis to be the axis of anisotropy we obtain

$$\left( \frac{\partial \omega}{\partial k_x}, \frac{\partial \omega}{\partial k_y} \right) = \sin \theta \cos \theta \frac{\nu_o k^2 (1 + \cos^2 \theta) - 2\Omega}{k} (\cos \phi, \sin \phi), \quad (5.8)$$

$$\frac{\partial \omega}{\partial k_z} = \frac{\nu_o k^2 \sin^2 \theta + 2\Omega}{k} \sin^2 \theta. \quad (5.9)$$

In contrast to the case of waves in a rotating fluid where the energy propagates perpendicularly to the wave-vector (along the axis of rotation) here the energy propagation direction has a component along the  $\mathbf{k}$  axis:

$$\frac{\partial \omega}{\partial \mathbf{k}} = \nu_o k \left\{ \hat{\mathbf{k}} (\hat{\mathbf{z}} \cdot \hat{\mathbf{k}}) \left[ 1 + (\hat{\mathbf{z}} \cdot \hat{\mathbf{k}})^2 \right] + \hat{\mathbf{z}} \left[ 1 - 3(\hat{\mathbf{z}} \cdot \hat{\mathbf{k}})^2 \right] \right\} + \frac{2\Omega}{k} \left[ \hat{\mathbf{z}} - \hat{\mathbf{k}} (\hat{\mathbf{z}} \cdot \hat{\mathbf{k}}) \right], \quad (5.10)$$

thus the group velocity is not perpendicular to the phase velocity (direction of propagation) in contradistinction to the rigidly-rotating liquid case. The modulus of the group velocity is

$$\left| \frac{\partial \omega}{\partial \mathbf{k}} \right| = \frac{\sin \theta \sqrt{5 (\cos^4 \theta) k^4 \nu_o^2 - 2k^2 \nu_o (k^2 \nu_o + 6\Omega) (\cos^2 \theta) + (k^2 \nu_o + 2\Omega)^2}}{k}. \quad (5.11)$$

In Fig. 7 we plot the group velocity magnitude (5.11) versus angle  $\theta$  (formed between the wavevector  $\mathbf{k}$  and the  $z$ - (rotation) axis, setting  $k = \nu_o = 1$ ).

The determinant of the second derivative of the dispersion relation  $\partial_{k_i k_j}^2 \omega$  becomes

$$|\partial_{k_i k_j}^2 \omega| = \frac{1}{k^6} \cos \theta \sin^2 \theta \left( 5k^4 \nu_o^2 \cos^4 \theta - 4\nu_o k^2 (k^2 \nu_o + 4\Omega) \cos^2 \theta - (k^2 \nu_o - 2\Omega)^2 \right) \times (k^2 \nu_o \cos^2 \theta + k^2 \nu_o - 2\Omega) \quad (5.12)$$

The extrema of the group velocity related to the roots of  $|\partial_{k_i k_j}^2 \omega|$  are displayed in Table 2. In its third line we recognize the group velocity  $\frac{k^2 \nu_o + 2\Omega}{k} \hat{\mathbf{z}}$  with energy propagating along the axis of rotation/anisotropy known from the literature (Davidson 2013; Kirkinis & Olvera de la Cruz 2023) when the wavevector is perpendicular to this axis ( $\theta = \pi/2$ ). From the first and second lines of the Table we however see that depending on the parameter values and signs for odd viscosity  $\nu_o$  and angular velocity  $\Omega$  there might be different wavenumber directions ( $\theta \neq \pi/2$ ) with the energy propagating along the axis or at an angle to it. The allowed parameter  $(\nu_o, \Omega)$  regions for the existence of the roots in Table 2 appear in Fig. 20.

### 5.1. Combined $\eta_4, \eta_o$ effects with $\Omega$ .

Apart from Eq. (2.1), there is also a second odd viscous (non-dissipative) constitutive law that may be employed to describe the properties of an odd viscous liquid (Lifshitz & Pitaevskii 1981, §58)

$$\boldsymbol{\sigma}' = \eta_4 \begin{pmatrix} 0 & 0 & -(\frac{1}{r} \partial_\phi v_z + \partial_z v_\phi) \\ 0 & 0 & \partial_r v_z + \partial_z v_r \\ -(\frac{1}{r} \partial_\phi v_z + \partial_z v_\phi) & \partial_r v_z + \partial_z v_r & 0 \end{pmatrix}. \quad (5.13)$$

Although combination of the two constitutive laws (2.1) and (5.13) with rigid-rotation of angular velocity  $\Omega$  is complicated, its consequences on fluid-flow behavior can be obtained by performing the substitution

$$\nu_o \rightarrow \nu_o - \nu_4, \quad \text{and} \quad 2\Omega \rightarrow 2\Omega + \nu_4 k^2 \quad (5.14)$$

in the results already obtained in section 2. This can be seen, for instance, from the reduced form of Eq. (2.8)

$$-i\omega v_r = -i \frac{\omega}{k^2} \mathcal{L} v_r - [(\nu_o - \nu_4) \mathcal{L} - 2\Omega - k^2] v_\phi, \quad (5.15)$$

$$-i\omega v_\phi = [(\nu_o - \nu_4) \mathcal{L} - 2\Omega - k^2] v_r \quad (5.16)$$

and this is exactly the form of the Navier-Stokes equations when both (2.1) and (5.13) are employed. Thus, considering velocity fields  $v_r, v_\phi \propto J_1(\kappa r)$  as in section 2, we obtain exactly the same type of  $\kappa$  roots as those described in Fig. 2 and Table 1 by making the substitution (5.14). We thus do not need to discuss this case further.

For plane polarized waves one can perform the substitution (5.14) and obtain the same results as in section 5 with the exception of the group velocity and higher order derivatives of  $\omega$  with respect to  $k_z$ . We briefly discuss the governing equations since they can be expressed in a concise form and lead to certain conclusions about the helicity of the flow. Another reason for wanting to discuss both odd viscosity coefficients  $\nu_o$  and  $\nu_4$  is that certain combinations have been employed in the literature to simplify the discussion cf. (Markovich & Lubensky 2021; Khain *et al.* 2022) and in particular the combination  $\eta_o = 2\eta_4$  which we call elliptic. Also the (parabolic) combination  $\eta_o = \eta_4$  simplifies the discussion significantly. The names elliptic or parabolic are inherited from the form obtained by the governing differential operator  $\mathcal{S}$  that will be defined below.

Expressing both odd stress tensors (2.1) and (5.13) in Cartesian coordinates we obtain

$$\boldsymbol{\sigma}' = \begin{pmatrix} -\eta_o(\partial_x v + \partial_y u) & \eta_o(\partial_x u - \partial_y v) & -\eta_4(\partial_y w + \partial_z v) \\ \eta_o(\partial_x u - \partial_y v) & \eta_o(\partial_x v + \partial_y u) & \eta_4(\partial_x w + \partial_z u) \\ -\eta_4(\partial_y w + \partial_z v) & \eta_4(\partial_x w + \partial_z u) & 0 \end{pmatrix}. \quad (5.17)$$

Let

$$\mathcal{S} = (\nu_o - \nu_4)\nabla_2^2 + \nu_4\partial_z^2. \quad (5.18)$$

With  $\zeta = \partial_x v - \partial_y u$  denoting the component of vorticity in the  $z$  direction and a modified pressure  $\tilde{p} = p + \eta_4\zeta$ , the Navier-Stokes equations of a rigidly-rotating liquid, characterized by the constitutive law (5.17), become

$$\frac{D\mathbf{v}}{Dt} = -\frac{1}{\rho}\nabla\tilde{p} + (\mathcal{S} - 2\Omega)\hat{\mathbf{z}} \times \mathbf{v}. \quad (5.19)$$

The linearized vorticity equation (5.1) is thus replaced by

$$\partial_t \text{curl} \mathbf{v} = -(\mathcal{S} - 2\Omega)\frac{\partial \mathbf{v}}{\partial z}. \quad (5.20)$$

With  $\mathbf{v} = \mathbf{A}e^{i(\mathbf{k}\cdot\mathbf{r} - \omega t)}$ , the dispersion relation becomes

$$\omega = \pm [2\Omega - \mathcal{S}(\mathbf{k})]\frac{k_z}{k} \quad \text{or} \quad \omega = \pm \cos\theta \left\{ k^2 [\nu_o - \nu_4 - (\nu_o - 2\nu_4)\cos^2\theta] + 2\Omega \right\} \quad (5.21)$$

where  $k = \sqrt{k_x^2 + k_y^2 + k_z^2}$  and

$$\mathcal{S}(\mathbf{k}) = -(\nu_o - \nu_4)(k_x^2 + k_y^2) - \nu_4 k_z^2. \quad (5.22)$$

The group velocity becomes

$$\left( \frac{\partial \omega}{\partial k_x}, \frac{\partial \omega}{\partial k_y} \right) = \pm \left[ k \left( (\nu_o - 2\nu_4)\cos^2\theta + \nu_o - \nu_4 \right) + 2\Omega \right] \sin\theta \cos\theta (\cos\phi, \sin\phi), \quad (5.23)$$

$$\frac{\partial \omega}{\partial k_z} = \pm k \left( (\nu_o - 2\nu_4)\cos^4\theta + (-2\nu_o + 5\nu_4)\cos^2\theta + \nu_o - \nu_4 \right) \pm 2\Omega. \quad (5.24)$$

As can be seen, the above relations simplify significantly in the limits  $\nu_o = 2\nu_4$  or  $\nu_o = \nu_4$ . The former recovers Eq. (8) of Markovich & Lubensky (2021),

$$\omega = \nu_4 k k_z + 2\Omega \frac{k_z}{k}, \quad (5.25)$$

now for an odd viscous liquid rotating rigidly with angular velocity  $\Omega$ .

Helicity is conserved for an odd viscous liquid that incorporates the constitutive law (5.17). We show this by considering the linearized vorticity equation (5.20) written in the form

$$-i\omega \mathbf{B} = i\mathbf{A}k_z [2\Omega - \mathcal{S}(\mathbf{k})], \quad (5.26)$$

when  $\text{curl} \mathbf{v} = \mathbf{B}e^{i(\mathbf{k}\cdot\mathbf{r} - \omega t)}$  and  $\mathcal{S}(\mathbf{k})$  is defined in Eq. (5.22). Since  $\omega = \pm [2\Omega - \mathcal{S}(\mathbf{k})]\frac{k_z}{k}$  (from (5.21)) we obtain  $\mathbf{B} = \mp k \mathbf{A}$ , or

$$\text{curl} \mathbf{v} = \mp k \mathbf{v}. \quad (5.27)$$

Thus, the helicity of the flow field determined by the odd stress tensor (5.17) is conserved

$$\mathbf{v} \cdot \text{curl} \mathbf{v} = \mp k |\mathbf{v}|^2 \quad (5.28)$$

which can be seen from the form of the velocity field (5.6) for  $\mathbf{a} \perp \mathbf{b}$ .

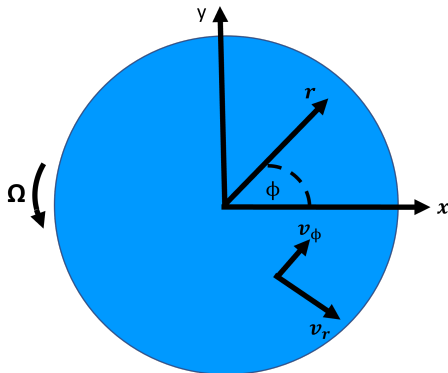


Figure 9: Two-dimensional odd viscous compressible liquid rotating with angular velocity  $\Omega$ . In plane polar coordinates the velocity field is  $\mathbf{v} = v_r \hat{\mathbf{r}} + v_\phi \hat{\boldsymbol{\phi}}$  in the frame rotating with the liquid at constant angular velocity  $\Omega$ .

## 6. Inertial oscillations in a rigidly-rotating compressible two-dimensional odd viscous liquid

### 6.1. Axisymmetric inertial waves

A two dimensional compressible liquid endowed with odd viscosity obeys the constitutive law (Lapa & Hughes 2014; Ganeshan & Abanov 2017)

$$\boldsymbol{\sigma}' = \eta_o \begin{pmatrix} -(\partial_r v_\phi - \frac{1}{r} v_\phi + \frac{1}{r} \partial_\phi v_r) & \partial_r v_r - \frac{1}{r} v_r - \frac{1}{r} \partial_\phi v_\phi \\ \partial_r v_r - \frac{1}{r} v_r - \frac{1}{r} \partial_\phi v_\phi & \partial_r v_\phi - \frac{1}{r} v_\phi + \frac{1}{r} \partial_\phi v_r \end{pmatrix}, \quad (6.1)$$

and the continuity equation

$$\partial_t \rho' + \rho \operatorname{div} \mathbf{v} = 0 \quad \text{for} \quad \rho' \ll \rho, \quad (6.2)$$

where  $\rho'$  is the variable part of the density and  $\rho$  a constant background level. As in section 2, consider an axisymmetric geometry, now described by plane polar coordinates  $r, \phi$  (cf. Fig. 9) the fields are independent of  $\phi$ , we neglect nonlinear terms (assuming small-amplitude motions) and the time dependence is given by the factor  $\exp[-i\omega t]$  where  $\omega$  is a real frequency. Employing the constitutive law (6.1), the linearized equations of motion become (Lifshitz & Pitaevskii 1981, §89)

$$-i\omega v_r = -\frac{c^2}{\rho} \frac{\partial \rho'}{\partial r} + 2\Omega v_\phi - \nu_o \left[ \frac{1}{r} \frac{\partial}{\partial r} \left( r \frac{\partial v_\phi}{\partial r} \right) - \frac{v_\phi}{r^2} \right], \quad (6.3)$$

$$-i\omega v_\phi = -2\Omega v_r + \nu_o \left[ \frac{1}{r} \frac{\partial}{\partial r} \left( r \frac{\partial v_r}{\partial r} \right) - \frac{v_r}{r^2} \right], \quad (6.4)$$

$$-i\omega \rho' = -\rho \frac{1}{r} \frac{\partial}{\partial r} (r v_r), \quad (6.5)$$

where  $c$  is the speed of sound. Because of Eq. (6.5) we obtain

$$\frac{\partial \rho'}{\partial r} = \frac{\rho}{i\omega} \frac{\partial}{\partial r} \left( \frac{1}{r} \frac{\partial}{\partial r} (r v_r) \right). \quad (6.6)$$

We again employ the identity  $\frac{\partial}{\partial r} \left( \frac{1}{r} \frac{\partial}{\partial r} (r v_r) \right) = \frac{1}{r} \frac{\partial}{\partial r} \left( r \frac{\partial v_r}{\partial r} \right) - \frac{v_r}{r^2}$ , and the linear operator  $\mathcal{L} = \partial_r^2 + \frac{1}{r} \partial_r - \frac{1}{r^2}$  we introduced in Eq. (2.7). The  $r$  and  $\phi$  momentum equations (6.3),

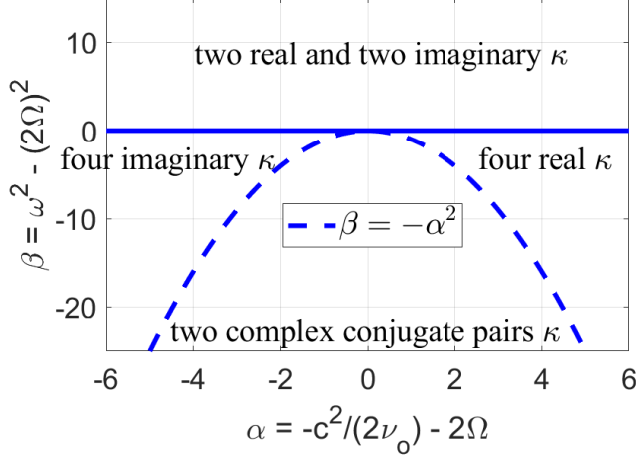


Figure 10: Roots of Eq. (6.10) in the parameter space  $(\alpha, \beta)$  defined in Eq. (6.12). Rich behavior exists in the presence of rotation. This includes the oscillatory Bessel functions for real  $\kappa$ , exponentially increasing/decreasing Bessel functions for  $\kappa$  imaginary and exponential-oscillating Bessel functions for complex  $\kappa$  (see Fig. 2 for the qualitative form of these Bessel functions)

(6.4) become

$$-i\omega v_r = -\frac{c^2}{i\omega} \mathcal{L} v_r - (\nu_o \mathcal{L} - 2\Omega) v_\phi, \quad (6.7)$$

$$-i\omega v_\phi = (\nu_o \mathcal{L} - 2\Omega) v_r. \quad (6.8)$$

Expressing the velocities  $v_r$  and  $v_\phi$  in terms of Bessel or modified Bessel functions,  $v_r = A J_1(\kappa r)$ ,  $v_\phi = B J_1(\kappa r)$ , or  $v_r = A I_1(\kappa r)$ ,  $v_\phi = B I_1(\kappa r)$ , etc., (where  $A$  and  $B$  are constants to be determined by the boundary conditions and  $\kappa$  is an eigenvalue) the system (6.7) and (6.8) has a solution when the determinant  $-\kappa^4 \nu_o^2 - 4\Omega \kappa^2 \nu_o - c^2 \kappa^2 - 4\Omega^2 + \omega^2$  of the coefficients of the resulting linear system

$$-\frac{i(-\kappa^2 \nu_o - 2\Omega) B \omega - A c^2 \kappa^2}{\omega^2} - A = 0, \quad \text{and} \quad \frac{iA(-\kappa^2 \nu_o - 2\Omega)}{\omega} - B = 0 \quad (6.9)$$

vanishes. Consider first the case where the origin is included in the domain. It is not difficult to show that the solution is the Bessel function  $J_1(\kappa r)$  for which  $\kappa$  satisfies

$$\kappa^2 = \frac{-4\Omega \nu_o - c^2 + \sqrt{8\Omega c^2 \nu_o + c^4 + 4\nu_o^2 \omega^2}}{2\nu_o^2}. \quad (6.10)$$

As with Eq. (2.12) of the three-dimensional case of section 2, Eq. (6.10) here is a relation between the allowed (possibly complex) eigenvalue  $\kappa$  and the (real) frequency  $\omega$ . We can cast Eq. (6.10) in a form resembling (2.12) and (2.14). Thus,

$$\nu_o \kappa^2 = -\frac{c^2}{2\nu_o} - 2\Omega \pm \sqrt{\left(-\frac{c^2}{2\nu_o} - 2\Omega\right)^2 + \omega^2 - (2\Omega)^2} \equiv \alpha \pm \sqrt{\alpha^2 + \beta} \quad (6.11)$$

where we carried-out the substitution

$$\alpha = -\frac{c^2}{2\nu_o} - 2\Omega, \quad \beta = \omega^2 - (2\Omega)^2, \quad (6.12)$$

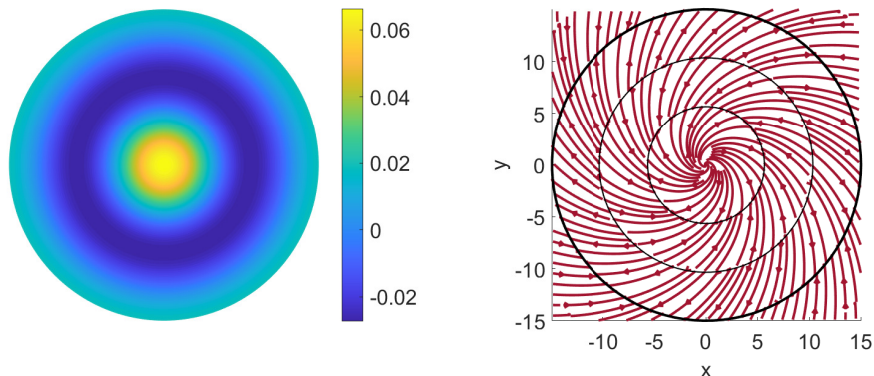


Figure 11: **Left panel:** Plot of the density  $\rho'$  in (7.2) for a two-dimensional compressible odd viscous liquid contained in a disk of radius  $b = \gamma_3/\kappa$  where  $\gamma_3 = 10.173$  is the third zero of the Bessel function  $J_1$ . **Right panel:** Instantaneous streamlines in the  $x-y$  plane of the velocity field  $v_r$  and  $v_\phi$  in (7.2), representing oscillations of an odd viscous liquid with frequency  $\omega$ . The liquid is contained in the disk denoted by the thick black circle. The two interior thin black circles have been included only as a guide to the eye and denote the location of the zeros of the Bessel function  $J_1$ , that is, the location where the velocity vanishes. For a liquid that extends beyond the disk, its streamlines are as shown in the region outside the thick black circle.

to be compared with the definition of  $\alpha$  and  $\beta$  in (2.13). Therefore the classification of the roots  $\kappa$  of Eq. (2.12) displayed in, Fig. 2 and Table 1, carry-over in the present section unchanged by making the substitution (6.12). We display the parameter regimes again in Fig. 6.12 with respect to the new meaning of the parameter  $\alpha$ .

Thus, overall we found that inertial waves in a compressible two dimensional and rigidly rotating odd viscous liquid exist and have the velocity fields and density

$$v_r = AJ_1(\kappa r)e^{-i\omega t}, \quad v_\phi = -iA \frac{2\Omega + \nu_o \kappa^2}{\omega} J_1(\kappa r)e^{-i\omega t}, \quad \rho' = -iA \frac{\rho \kappa}{\omega} J_0(\kappa r)e^{-i\omega t} \quad (6.13)$$

and these resemble their three-dimensional counterparts of Eq. (2.15).

## 7. Illustrative examples

### 7.1. Inertial oscillations of a two-dimensional odd viscous liquid in a disk

Consider the case where  $\omega \sim 2\Omega$  and thus  $\nu_o \kappa^2 \sim 2\alpha = 2\left(-\frac{c^2}{2\nu_o} - 2\Omega\right)$  or  $\nu_o \kappa^2 = 0$  from Eq. (6.11). Two real roots exist as long as  $4\Omega < -c^2/\nu_o$  and the velocity field is given by (6.13). This motion comprises regions between concentric circles of radius  $r_n$  such that

$$r_n \kappa = \gamma_n \quad (7.1)$$

and  $\gamma_n$  are the zeros of  $J_1(x)$ . Both  $v_r$  and  $v_\phi$  vanish at these concentric circles and the fluid does not cross them. Introducing the polar form for the amplitude  $A = ae^{i\theta}$ , where  $a$  and  $\theta$  are real amplitude and phase, we can cast the complex fields of (6.13) in real

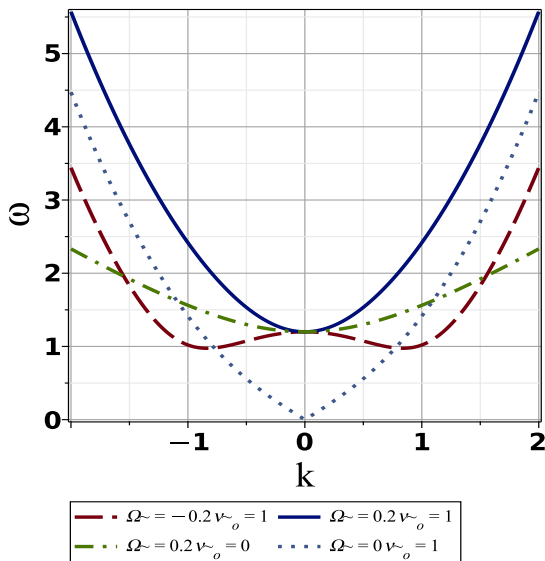


Figure 12: Dispersion relation (7.6) versus wavenumber  $k = k_x$  (evaluated at  $k_y = 0$  for clarity). Of primary interest is the dashed curve denoting the existence of non-convex dispersion for the displayed parameters ( $\Omega\nu_o < 0$ ). At its inflection points the corresponding group velocity attains its maximum value (cf. Fig. 13) and the second derivative  $|\partial_{k_i k_j}^2 \omega|$  vanishes (cf. Fig. 14), implying the presence of caustics and a breakdown of the longtime asymptotics. The dotted line ( $\Omega = 0, \nu_o \neq 0$ ) is also of interest since the dispersion curve develops a cusp at  $k = 0$ . Thus, the group velocity develops a jump as one traverses  $k_x$  from negative to positive values (cf. Fig. 13).

form

$$v_r = aJ_1(\kappa r) \cos(\theta - \omega t), \quad v_\phi = a \frac{2\Omega + \nu_o \kappa^2}{\omega} J_1(\kappa r) \sin(\theta - \omega t), \quad \rho' = a \frac{\rho \kappa}{\omega} J_0(\kappa r) \sin(\theta - \omega t). \quad (7.2)$$

We consider the liquid confined within a solid cylindrical surface located, say, at  $r = b$ , that would be realistic in a laboratory setting. This boundary will be a streamline located at an integral number of cells in the radial direction. If by  $\gamma_n$  we denote the  $n$ -th zero of the Bessel function  $J_1$ , Eq. (6.11) with the condition  $\kappa b = \gamma_n$  lead to the constraint

$$b \left( \frac{-4\Omega\nu_o - c^2 + \sqrt{8\Omega c^2\nu_o + c^4 + 4\nu_o^2\omega^2}}{2\nu_o^2} \right)^{1/2} = \gamma_n \quad (7.3)$$

and  $n$  denotes the number of cells in the radial direction (cf. Fig. 4). From Eq. (7.3) one can relate the frequency of oscillation  $\omega$  with the cylinder radius  $b$

$$\omega^2 = (\nu_o \kappa^2 + 2\Omega)^2 + (c\kappa)^2, \quad \kappa = \frac{\gamma_n}{b}, \quad (7.4)$$

where  $n$  denotes the number of cells in the radial direction.

In Fig. 11 we plot the density  $\rho'$  in (7.2) when the liquid is contained in a disk of radius  $b = \gamma_3/\kappa$  where  $\gamma_3 = 10.173$  is the third zero of the Bessel function  $J_1$  and the corresponding instantaneous streamlines of the velocity field  $v_r$  and  $v_\phi$  in (7.2). The streamlines contained between two adjacent concentric circles change direction periodically with period  $T = 2\pi/\omega$ .

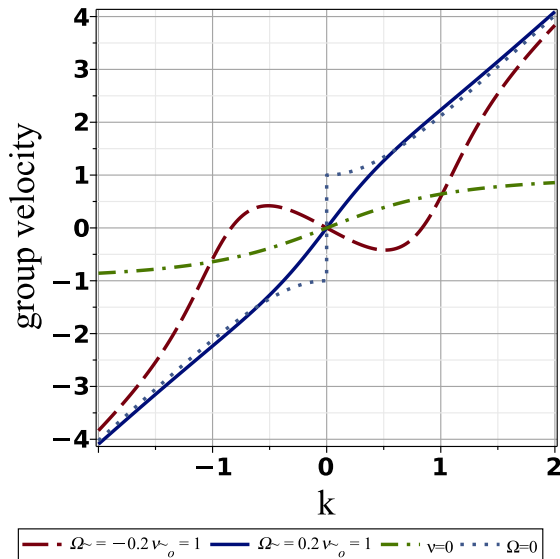


Figure 13:  $k = k_x$  component of the group velocity (7.7) (setting  $k_y = 0$  for clarity). Of interest is the dashed curve for the indicating parameter values, which attains local maxima and minima corresponding to the inflexion points of the dispersion relation (cf. Fig. 12) and the vanishing of the determinant second derivative  $|\partial_{k_i k_j}^2 \omega|$  (cf. Fig. 14), indicating the presence of caustics (overlapping of space-time rays (Ostrovsky & Potapov 1999, Fig. 6.3)). Of interest is also the dotted line (odd viscosity in the absence of rotation) which displays a jump at  $k = 0$ .

## 7.2. Polarized waves

When the wavenumber  $\kappa$  in (7.4) is real one can develop the counterpart of the three-dimensional plane polarized waves of section 5. The important point is that for certain parameter regimes the dispersion relation (7.4) can become non-convex. At an inflection point of the dispersion relation (7.4) the group velocity is maximum and the determinant of  $\partial_{k_i} \partial_{k_j} \omega$  vanishes. This implies that rays (characteristics) of the nonlinear transport equation  $\partial_t \omega + \mathbf{c}_g(\omega) \cdot \nabla \omega = 0$  carrying an initial frequency profile, overlap at a specific interval of space and time giving rise to a caustic curve (Lighthill 1978; Ostrovsky & Potapov 1999). Although this behavior is still physically realistic, the ray theory (where slow variations of wavenumber are assumed) employed to calculate Fourier integrals in wavenumber space breaks down; the method of stationary phase breaks down and one needs to calculate these Fourier integrals by using higher order derivatives of  $\omega$  with respect to  $\mathbf{k}$  (usually third order derivatives). When nonlinear terms are added to these linear systems, unusual behavior is observed such as oscillatory soliton tails and dispersive shocks (Lowman & Hoefler 2013; Sprenger & Hoefler 2017) arising as radiation due to motion of the medium emanating when the velocity of particles moving in it is larger than the phase velocity of waves that propagate in this medium (Cherenkov radiation, cf, (Landau & Lifshitz 1960; Kuznetsov & Dias 2011)). Here we will not pause to display these nonlinear effects, most of which are well-known in the literature. We will establish the existence of planar inertial waves and discuss the behavior of the dispersion that may give rise to the aforementioned effects.

Let  $\psi = k_1 v_2 - k_2 v_1$  and  $\chi = k_1 v_1 + k_2 v_2$ . Thus,  $\psi = \text{curl} \mathbf{v}^t$  (in coordinate space) and  $\chi = \text{div} \mathbf{v}^l$  are the derivatives of the transverse and longitudinal velocity components,

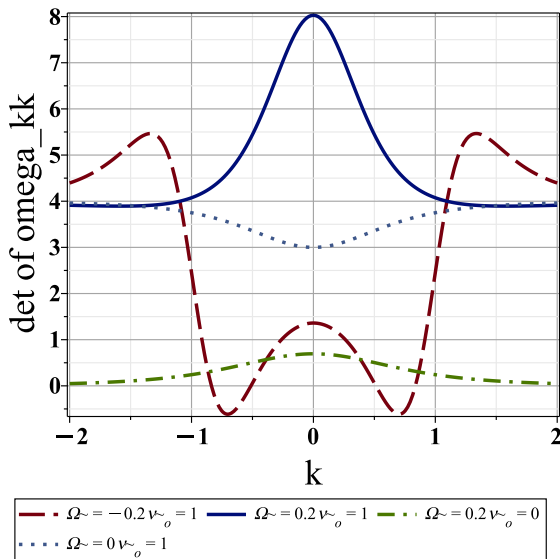


Figure 14: Determinant of the matrix  $\partial_{k_i k_j}^2 \omega$  in (7.8) vs.  $k = k_x$  (setting  $k_y = 0$  for compatibility with the two previous figures). Of interest is the dashed curve for the indicating parameter values, which vanishes near  $k_x \sim \pm 0.5$  corresponding to the inflexion points of the dispersion relation (cf. Fig. 12) and the extrema of the group velocity (cf. Fig. 13), indicating the presence of caustics (overlapping of space-time rays (Ostrovsky & Potapov 1999, Fig. 6.3)).

respectively. Then, we can replace the momentum equations with two equations for  $\chi$  and  $\psi$  (see for instance (Landau & Lifshitz 1980, §89))

$$\frac{d\chi}{dt} = -ik^2 c^2 \frac{\rho'}{\rho} + (2\Omega + \nu_o k^2)\psi, \quad \frac{d\psi}{dt} = -(2\Omega + \nu_o k^2)\chi, \quad \frac{d\rho'}{dt} = -i\rho\chi \quad (7.5)$$

where we employed the notation  $\chi, \rho$  and  $\psi$  to denote quantities in both coordinate and momentum representation. We can derive a single second order linear oscillator equation for  $\chi$ , namely  $\frac{d^2\chi}{dt^2} + \omega^2\chi = 0$ , where

$$\omega^2 = (kc)^2 + (2\Omega + \nu_o k^2)^2, \quad \text{for } k = \sqrt{k_x^2 + k_y^2}. \quad (7.6)$$

The group velocity associated with dispersion (7.4) becomes

$$\mathbf{c}_g = \frac{(2k^2\nu_o^2 + \tilde{c}^2)}{\sqrt{k^4\nu_o^2 + \tilde{c}^2k^2 + 4\Omega^2}}(k_x, k_y) \quad (7.7)$$

where  $\tilde{c}^2 = 4\Omega\nu_o + c^2$  whose significance will be discussed in section 7.3, and the determinant of the matrix  $\partial_{k_i k_j}^2 \omega$  is

$$|\partial_{k_i k_j}^2 \omega| = \frac{[2k^2\nu_o^2(\nu_o^2k^4 + 12\Omega^2) + \tilde{c}^2(3\nu_o^2k^4 + 4\Omega^2)](2k^2\nu_o^2 + \tilde{c}^2)}{(k^4\nu_o^2 + \tilde{c}^2k^2 + 4\Omega^2)^2}, \quad (7.8)$$

and comparison of (7.7) with (7.8) shows that they share a common zero.

With respect to the dashed curve in Figures 12-14, representing the dispersion, group velocity and second derivative of dispersion of a rigidly-rotating odd viscous liquid with  $\Omega\nu_o < 0$  we point-out the following characteristics.

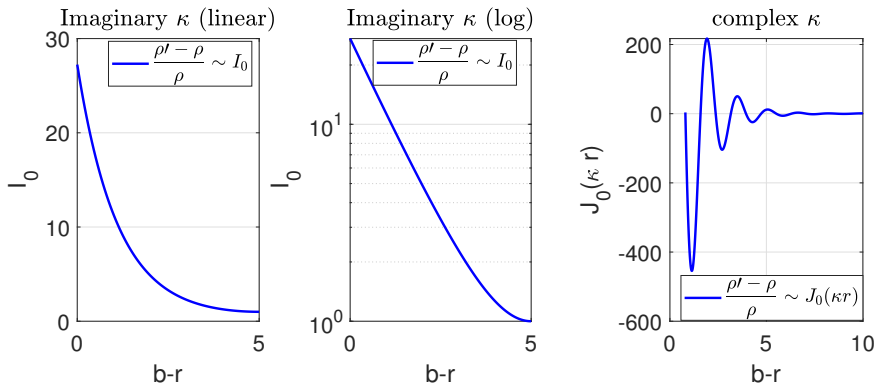


Figure 15: Theoretical qualitative predictions of the model (6.3)-(6.5) for the behavior of the density  $\rho'$  in (7.2) of a compressible odd viscous liquid in a disk. Left two panels (Case I of Table 3): Density for imaginary  $\kappa$ , displayed in linear and logarithmic vertical axes respectively, obtained as solution of Eq. (6.11). The horizontal axis denotes distance from a circular boundary located at  $r = b$ . When  $\kappa$  is complex, the rightmost panel (Case II of Table 3) gives the characteristic behavior of the density. These profiles are to be compared with the numerical results of (Souslov *et al.* 2019) displayed in their Fig. 3(b) and 3(d). Thus, the density profile resembles an evanescent wave (see discussion at the end of section 7.3).

(i) At the inflection point of the dispersion curve (7.6) the group velocity is maximum and  $|\partial_{k_i k_j}^2 \omega|$  vanishes.

(ii) At the bottom of the well (the minimum of the dispersion curve) in (7.6) the group velocity vanishes and  $|\partial_{k_i k_j}^2 \omega|$  vanishes as well.

With respect to the dotted curve in Figures 12-13, representing the dispersion and group velocity of a rigidly-rotating odd viscous liquid with  $\Omega \equiv 0$  we point-out the following characteristics.

(i) The dispersion curve (7.6) has a cusp at  $k = 0$ ,  $\omega \sim c|k|$ .

(ii) The group velocity is equal to  $\mp c$ , as we approach the  $k = 0$  line from the left (negative sign) and the right (positive sign).

The determinant  $|\partial_{k_i k_j}^2 \omega|$  in (7.8) vanishes at two locations as indicated in Fig. c. First, at the zero  $k^2 = \frac{4\Omega\nu_o + c^2}{-2\nu_o^2}$  it shares with the group velocity, and second at

$$k^2 = \frac{\left(4c^{\frac{2}{3}}\Omega\nu_o + c^{\frac{8}{3}}\right) (8\Omega\nu_o + c^2)^{\frac{2}{3}} + c^4 + 8\Omega c^2\nu_o + c^{\frac{4}{3}} (8\Omega\nu_o + c^2)^{\frac{4}{3}}}{-2(8\Omega\nu_o + c^2)^{\frac{2}{3}} c^{\frac{2}{3}} \nu_o^2}. \quad (7.9)$$

Only specific values of the parameters give rise to real observables in these relations. In Fig. 19 we display the roots of Eq. (7.9) and the modulus of the group velocity (7.7) for the allowed combination of parameters  $\Omega$  and  $\nu_o$ .

### 7.3. Topologically protected waves

The analysis of section 6.1 can be applied to describe the behavior of density waves away from a solid boundary. In (Souslov *et al.* 2019, Eq. (3)) the dispersion relation (7.4) for real wavenumber  $(k_x, k_y)$  is derived in a Cartesian representation of the momentum and continuity equations and show (numerically) the existence of waves that propagate unidirectionally in the vicinity of a circular boundary, with a single obstacle, circumscribing a two dimensional compressible odd viscous liquid (referred to as cases I & II in

---

	$c$	$\Omega$	$\nu_o$	$\rho$	$\alpha$	$\alpha^2 + \beta$	Effect	Renormalized $c$
Case I	8	-20	0.1	1	-280	$\omega^2 + 76800$	no scattering	$\tilde{c}_I = 7.48$
Case II	15	-500	2	1	$3775/4$	$\omega^2 - 1749375/16$	no scattering	
Case III	8	20	0.1	1	-360	$\omega^2 + 128000$	scattering	$\tilde{c}_{III} = 8.48$

---

Table 3: Parameter values  $(c, \Omega, \nu_o, \rho)$  employed in (Souslov *et al.* 2019) to numerically demonstrate the existence of topological waves.  $\alpha$  and  $\beta$  are the parameters defined in Eq. (6.12) to classify the system behaviors displayed in Fig. 10. Parameter Cases I & II above leading to radial Navier-Stokes eigenvalues  $\kappa$  obtained as roots of Eq. (6.10), are displayed in the left and right panel of Fig. 16, respectively, for arbitrary value of the frequency  $\omega$ . Odd viscosity coupled to rigid rotation renormalizes the speed of sound of the medium and leads disturbances to propagate with supersonic (no scattering from a solid obstacle) or subsonic (scattered from a solid obstacle) speed, cf. Fig. 17.

---

the present paper). It is possible to employ the formulation developed in section 6.1 to reach certain conclusions about the structure of the velocity and density fields, based on the general parameter  $\kappa$  whose character was analysed in Eq. (6.11) and Fig. 10.

In (Souslov *et al.* 2019) three parameter regimes are chosen to demonstrate three distinct behaviors, the first two giving rise to unidirectional wave propagation along the circular boundary. We tabulate the material parameters of these two cases in Table 3. In case I, the first set of values  $(c, \Omega, \nu_o, \rho) = (8, -20, 0.1, 1)$  gives in our parametric representation

$$(\alpha, \alpha^2 + \beta) = (-280, \omega^2 + 76800), \quad (7.10)$$

which implies that equations (6.10) or (6.11) have four imaginary roots  $\kappa$ , by looking at the diagram in Fig. 10 (for  $\omega \equiv 0$  these are  $\kappa \sim \pm 5.36i, \pm 74.64i$ ). Thus, the exponentially increasing (from the origin of the disk) solution representing the density  $\rho'$  of the liquid will have, in the radial direction, the form of the modified Bessel function  $I_0$ . We display in the left two panels of Fig. 15 the modified Bessel function  $I_0$  in linear and logarithmic vertical axes, as a function of the radial coordinate  $b - r$ , that is, measuring distance from a boundary located at  $r = b$ . These two panels qualitatively capture the two graphs of Figure 3(b) in (Souslov *et al.* 2019) giving rise to the protected density waves of Fig. 3(a) of the same reference.

For completeness we display in Fig. 16a the frequency  $\omega$  plotted against the real and imaginary parts  $\kappa_1$  and  $\kappa_2$  respectively, of  $\kappa = \kappa_1 + i\kappa_2$ . When  $\beta < 0$  ( $\omega < 2|\Omega| = 40$ ), the four imaginary roots are clearly visible. When  $\beta$  becomes positive,  $\kappa$  changes character and Eq. (6.10) acquires two real and two imaginary  $\kappa$  roots as is evident in Fig. 16a.

We repeat the above analysis for the second set of parameters employed in the analysis of (Souslov *et al.* 2019)  $(c, \Omega, \nu_o, \rho) = (15, -500, 2, 1)$ , since there is some interesting qualitative behavior that can also be captured by our analysis. The parametric space implied by Fig. 10 becomes in this case

$$(\alpha, \alpha^2 + \beta) = (3775/4, \omega^2 - 1749375/16). \quad (7.11)$$

It can be seen from Eq. (6.11) that the roots can be complex conjugate pairs, all real or two real and two imaginary. For small  $\omega \sim 0$  (as was considered in (Souslov *et al.* 2019)) we obtain two complex conjugate pairs (for  $\omega \equiv 0$  these are  $\kappa = \pm 5\sqrt{151 \pm 3i\sqrt{311}}/2$ ). Now the density  $\rho'$  of the liquid will have, in the radial direction, the form of the modified Bessel function  $J_0(\kappa r)$  for complex  $\kappa$ . We display in the rightmost panel of Fig. 15 the

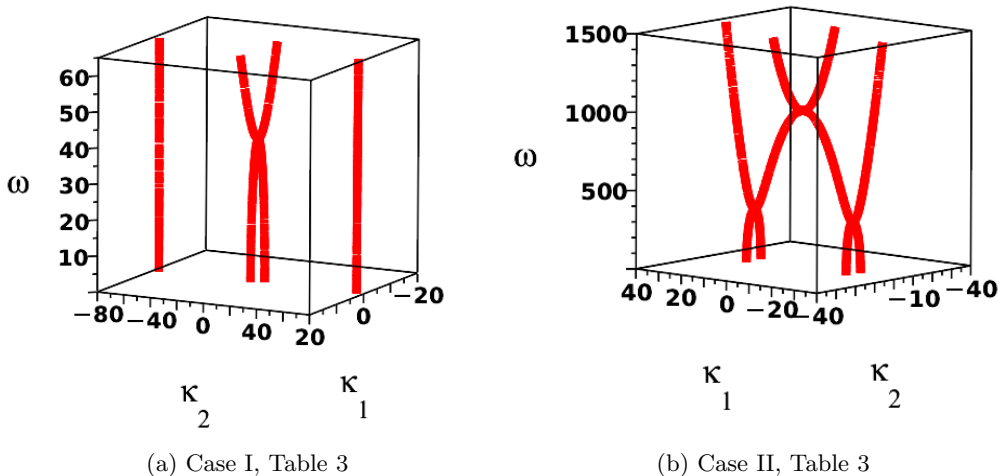


Figure 16: Real frequency  $\omega$  versus the real  $\kappa_1$  and imaginary part  $\kappa_2$  of the eigenvalue  $\kappa = \kappa_1 + i\kappa_2$  derived as solution of Eq. (6.10). Left panel: Bifurcation diagram for the first set of values  $(c, \Omega, \nu_o, \rho) = (8, -20, 0.1, 1)$  employed by (Souslov *et al.* 2019). As discussed in section 7.3, there are either four imaginary  $\kappa$ 's or two real and two imaginary for this set of values. The imaginary  $\kappa$ 's are associated with the evanescent wave form of the density as displayed in the left two panels of figure 15. When  $\omega = 0$  there are four imaginary  $\kappa$ 's. Right panel: Same diagram but for the values  $(c, \Omega, \nu_o, \rho) = (15, -500, 2, 1)$  of (Souslov *et al.* 2019). For  $\omega \equiv 0$  they are two pairs of complex conjugates associated with the evanescent wave form of the density as displayed in the rightmost panel of figure 15.

real part of the Bessel function  $J_0(\kappa r)$ , as a function of the radial coordinate  $b-r$ , that is, measuring distance from a boundary located at  $r = b$ . Although the density is restricted by an exponentially decaying envelope, it also oscillates (characteristic behavior of the Kelvin functions). Thus, the right-most panel of Fig. 15 qualitatively captures Figure 3(d) in (Souslov *et al.* 2019) giving rise to the protected density waves of Fig. 3(b) of the same reference. This oscillatory behavior is most visible in the video provided by (Souslov *et al.* 2019).

For completeness we display in Fig. 16b the frequency  $\omega$  plotted against the real and imaginary parts  $\kappa_1$  and  $\kappa_2$  respectively, of  $\kappa = \kappa_1 + i\kappa_2$ . When  $\beta < 0$  ( $\omega < 2|\Omega| = 1000$ ), two distinct behaviors are visible. Those that make  $\alpha^2 + \beta$  in (6.11) negative, giving rise to the aforementioned complex roots (located inside the parabola of Fig. 10), while those that make  $\alpha^2 + \beta$  positive give rise to four real roots (located outside the parabola of Fig. 10). When  $\beta$  becomes positive ( $\omega > 2|\Omega| = 1000$ ), we obtain two imaginary and two real roots for  $\kappa$ . It is clear that Figures 16a and 16b give rise to the continuous and dashed lines of Fig. 12 when  $\kappa$  becomes real (but miss the imaginary roots when these are present).

There is also a third case of material parameters considered in (Souslov *et al.* 2019) where  $\Omega\nu_o > 0$  (note that although the dispersion curve becomes non-convex when  $\Omega\nu_o < 0$  and  $k_x, k_y$  are real in Eq. (7.6), here the wavenumber is imaginary and the significance of the sign of  $\nu_o\Omega$  reverses since now  $\omega^2 = (-\nu_o\tilde{\kappa}^2 + 2\Omega)^2 - c^2\tilde{\kappa}^2$  for  $\kappa = i\tilde{\kappa}$  with  $\tilde{\kappa}$  being a real number. The essential features of this dispersion relation are displayed in Fig.16a). We tabulate the material parameters in Table 3. Thus, in case III, the set of

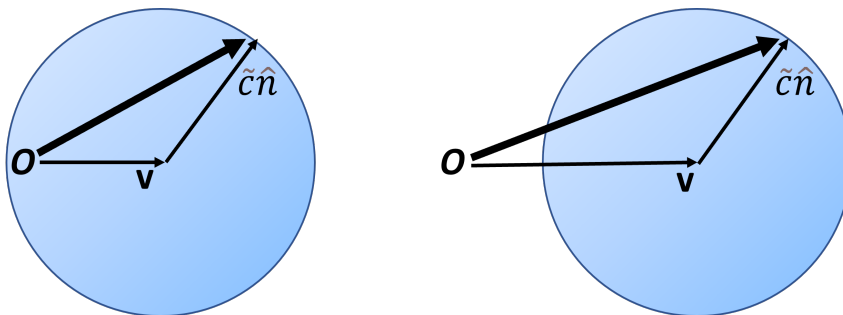


Figure 17: Explanation of scattering (case III), left panel, and non-scattering (case I), right panel, of topological waves from an obstacle in a two-dimensional compressible rigidly-rotating odd viscous liquid (Souslov *et al.* 2019). A subsonic disturbance ( $v < \tilde{c}$ ) at point  $O$  propagates with velocity  $\mathbf{v} + \tilde{c}\hat{\mathbf{n}}$  along the surface of the sphere depicted on the left, and eventually reaches any point in the medium ( $\mathbf{v}$  is the velocity of the medium,  $\hat{\mathbf{n}}$  a unit vector and  $\tilde{c}$  the renormalized speed of sound, see Eq. (7.14)). Likewise, a subsonic flow meeting an obstacle will be affected both upstream and downstream. This corresponds to case III of Table 3. On the other hand a supersonic disturbance  $v > \tilde{c}$  at point  $O$  can only propagate downstream within the cone depicted on the right. Likewise, a supersonic flow meeting an obstacle will only propagate downstream. This corresponds to case I of Table 3. The discussion is adopted from (Landau & Lifshitz 1987, §82). Compare with (Landau & Lifshitz 1987, Fig. 50).

values  $(c, \Omega, \nu_o, \rho) = (8, 20, 0.1, 1)$  gives in our parametric representation

$$(\alpha, \alpha^2 + \beta) = (-280, \omega^2 + 128000), \quad (7.12)$$

which implies that equations (6.10) or (6.11) have four imaginary roots  $\kappa$ , by looking at the diagram in Fig. 10 (for  $\omega \equiv 0$  these are  $\kappa \sim \pm 4.72i, \pm 84.72i$ ). Thus, the exponentially increasing (from the origin of the disk) solution representing the density  $\rho'$  of the liquid will have, in the radial direction, the form of the modified Bessel function  $I_0$ . Its bifurcation diagram is analogous to the one of Fig. 16a and it is not displayed.

There are however, qualitative differences between case I and case III. In case I one visually determines waves that do not scatter off from an obstacle, while in case III the waves scatter (Souslov *et al.* 2019, SI-movie). We thus proceed to provide an alternative explanation to the topological numbers argument of (Souslov *et al.* 2019) for the above behavior. Rewrite the dispersion relation in the form

$$\omega^2 = \nu_o^2 \tilde{\kappa}^4 - [4\nu_o\Omega + c^2] \tilde{\kappa}^2 + 4\Omega^2, \quad (7.13)$$

where for cases I & III  $\kappa = i\tilde{\kappa}$ ,  $\tilde{\kappa}$  being a real number. The speed of sound in the medium has been renormalized by odd viscosity and the angular velocity  $\Omega$ . Thus, let

$$\tilde{c} = \sqrt{4\nu_o\Omega + c^2}, \quad (7.14)$$

be the renormalized speed of sound. For case I  $\tilde{c}_I = 7.48$  (since  $\Omega\nu_o < 0$ ) and for case III  $\tilde{c}_{III} = 8.48$  ( $\Omega\nu_o > 0$ ). A disturbance propagating with a speed lying between these two values, moves with supersonic speed in the medium of case I, while it moves with subsonic speed in the medium of case III. Supersonic flow is distinctly different than subsonic flow. A disturbance of the latter flow eventually reaches every point in the medium. Likewise, the presence of an obstacle will affect the subsonic flow both upstream and downstream. On the other hand, a disturbance in supersonic flow propagates only downstream and lies within a cone, while the flow outside the cone remains unaffected. Likewise, when

supersonic flow meets an obstacle, it propagates downstream leaving the upstream region unaffected; the upstream region does not “know” about the presence of the obstacle. Fig. 17 displays these two distinctive behaviors and is adopted from (Landau & Lifshitz 1987, Fig. 50). These are predictions of linear analysis with axial symmetry and are expected to become somewhat modified in the presence of nonlinear and azimuthally-dependent fields. This is discussed now in terms of the liquid vorticity.

From (7.2) we can calculate the vorticity  $\text{curl}\mathbf{v} = \frac{1}{r} \frac{\partial(rv_\phi)}{\partial r} \hat{\mathbf{z}}$  of the two dimensional odd viscous liquid which is found to be proportional to the density  $\rho'$ :

$$\text{curl}\mathbf{v} = (\kappa^2\nu_o + 2\Omega)a\frac{\kappa}{\omega}J_0(\kappa r)\sin(\theta - \omega t)\hat{\mathbf{z}} = (\kappa^2\nu_o + 2\Omega)\frac{\rho'}{\rho}\hat{\mathbf{z}} \quad (7.15)$$

and this proportionality was also pointed-out in the numerical simulations of (Souslov *et al.* 2019, Fig. S2). So the question arises, why does the linear system of equations (6.3)-(6.5) giving rise to (7.15) agrees with the numerical predictions of (Souslov *et al.* 2019) who employ the nonlinear equations. The answer is that, although Eq. (7.15) can be thought of as being a consequence of the linearity of the governing equations, it is actually expected, from general grounds, that it will persist even when (the neglected here) nonlinear terms are incorporated into the Navier-Stokes equations (Pelz *et al.* 1985). This was indeed observed in the numerical solutions of the full Navier-Stokes equations performed in (Souslov *et al.* 2019, Fig. S2).

The two behaviors we’ve just analyzed, that is, exponentially decreasing waves away from a boundary, can be understood as being inertial *evanescent* waves (Nosan *et al.* 2021). As we showed in section 3.2, these are waves that are localized in the vicinity of a boundary and fall-off exponentially away from it.

When  $\omega \equiv 0$ , as in (Souslov *et al.* 2019, Fig.3), the system (6.3)-(6.5) simplifies significantly. We obtain

$$\frac{c^2}{\rho} \frac{\partial \rho'}{\partial r} = (\mathcal{L} - 2\Omega)v_\phi, \quad 0 = (\mathcal{L} - 2\Omega)v_r, \quad \partial_r(rv_r) = 0. \quad (7.16)$$

The last two equations imply that  $v_r \equiv 0$  everywhere. Thus, the azimuthal velocity  $v_\phi$  is modulated by the radial variation of an initial density distribution  $\rho'_0(r)$ . Letting  $\rho'_0(r) = \rho'_0 J_0(\kappa r)$  to be this distribution, one obtains from the first of (7.16) that

$$v_\phi = -\frac{\rho'_0}{\rho} \frac{\kappa c^2}{\nu_0 \kappa^2 + 2\Omega} J_1(\kappa r). \quad (7.17)$$

The direction of the azimuthal component of the velocity depends critically on the sign of  $\frac{\rho'_0 \kappa}{\nu_0 \kappa^2 + 2\Omega}$ .

Finally, depending on the type of the liquid (whether shear viscosity is included or not) there will be a boundary layer that will bring a velocity component, increasing exponentially in the bulk abruptly, down to zero near the boundary. We do not discuss here the manner by which this decay will take place and it is left for future investigations.

## 8. Discussion

In this paper we have brought forward a rather technical disambiguation of the various behaviors inertial-like waves of a rigidly-rotating odd viscous liquid can sustain. The presence of inertial-like waves and other oscillatory behavior that has appeared in recent literature of odd viscous liquids are due to the fact that these liquids are endowed with a restoring mechanism, some type of “elasticity”, similar to the restoring property of Coriolis forces (Batchelor 1967, §7.6) in an non-odd but rigidly-rotating viscous liquid.

The effects on a rigidly-rotating odd viscous liquid can be understood as a competition between the spatially-dependent odd frequency  $\Omega_o = \nu_o k^2$  and the angular velocity of the liquid  $\Omega$ , which leads to some unconventional behaviors. In three dimensions this includes the vanishing of the oscillation frequency at various wave-numbers and the loss of convexity of the dispersion relation. The flow field is of Beltrami type (vorticity parallel to velocity) and plane polarized waves conserve helicity. In two dimensions a compressible rotating odd viscous liquid shows a behavior analogous to its three dimensional counterpart since the governing equations (2.8) & (2.9), (5.15) & (5.16) and (6.7) & (6.8) are nearly identical and this is also corroborated by the form of the Bessel function eigenvalue  $\kappa$  in both cases Eq. (2.14) and (6.11) and their respective root diagrams Fig. 2 and 10.

In regions of low dissipation, as the one considered here, the velocity and vorticity show a tendency to align even when *nonlinear* terms of the Navier-Stokes equations are included in the analysis (Pelz *et al.* 1985). We expect that this alignment will persist when nonlinear terms will be included in the Navier-Stokes equations of an odd viscous liquid. In the two-dimensional compressible case this should lead to persistence of proportionality between vorticity and density. Effects of shear viscosity in odd stress-induced inertial waves are expected to follow familiar lines of rotating liquids (Chandrasekhar 1961).

Rotating and stratified Boussinesq flow can be decomposed in parameter regimes depending on the combination of strengths of these two effects (Embid & Majda 1998; Whitehead & Wingate 2014). The typical characteristic of these systems is the existence of a two-dimensional slow manifold towards which energy is being transferred due to fluctuations. Such a two-dimensional manifold is expected to exist in the case of a rigidly-rotating odd viscous liquid although the particle paths of odd viscous liquids are circular while those of internal gravity waves are rectilinear (Maas 2001).

A number of questions we have not attempted to answer concerns the application of boundary conditions. The odd viscous flow equations differ from their rigidly-rotating counterparts since the former are fourth order in the spatial derivatives, while the latter of second order. In the absence of shear viscosity it is unclear what conditions to consider. Here we circumvent this question by employing special parameter values.

Attempting to simplify the discussion we have considered the case of axially symmetric geometries where the flow is independent of the azimuthal angle  $\phi$ . More generally one can look for waves that display some form of periodicity in the azimuthal direction, so that the velocity field is proportional to a factor of the form  $e^{-im\phi}$  for integer  $m$  (Lopez & Marques 2016).

Finally, in the present and in past studies we have considered geometries where an eigenfunction expansion of the observables was always possible to carry-out. Real systems however, such as a sloping beach say, do not display such symmetries. In a series of experiments and theory (Maas 2001; Manders & Maas 2003) it was shown that two-dimensional wave attractors form due to wave focusing when they are reflected at a sloping boundary. We expect that similar patterns will appear in an odd viscous liquid, although in the absence of shear viscosity one would have to address first the type of boundary conditions the velocity field satisfies at a solid wall.

### Acknowledgments

This research was supported by the Center for Bio-Inspired Energy Science, an Energy Frontier Research Center funded by the US Department of Energy, Office of Science, Basic Energy Sciences under Award No. DE-SC0000989.

### Declaration of Interests

The authors report no conflict of interest.

## REFERENCES

- AVRON, J.E. 1998 Odd viscosity. *Journal of Statistical Physics* **92** (3-4), 543–557.
- AVRON, J.E., SEILER, R. & ZOGRAF, P.G. 1995 Viscosity of quantum Hall fluids. *Physical Review Letters* **75** (4), 697.
- BATCHELOR, G. K. 1967 *An introduction to fluid dynamics*. Cambridge: Cambridge University Press.
- CHANDRASEKHAR, S. 1961 *Hydrodynamic and hydromagnetic stability*. Oxford University Press.
- DAVIDSON, P.A. 2013 *Turbulence in rotating, stratified and electrically conducting fluids*. Cambridge University Press, Cambridge.
- EMBED, P.F. & MAJDA, A.J. 1998 Low Froude number limiting dynamics for stably stratified flow with small or finite Rossby numbers. *Geophysical & Astrophysical Fluid Dynamics* **87** (1-2), 1–50.
- GANESHAN, S. & ABANOV, A.G. 2017 Odd viscosity in two-dimensional incompressible fluids. *Physical Review Fluids* **2** (9), 094101.
- KHAIN, T., SCHEIBNER, C., FRUCHART, M. & VITELLI, V. 2022 Stokes flows in three-dimensional fluids with odd and parity-violating viscosities. *Journal of Fluid Mechanics* **934**, A23.
- KIRKINIS, E. 2023 Null-divergence nature of the odd viscous stress for an incompressible liquid. *Physical Review Fluids* **8** (1), 014104.
- KIRKINIS, E. & ANDREEV, A.V. 2019 Odd viscosity-induced stabilization of viscous thin liquid films. *Journal of Fluid Mechanics* **878**, 169–189.
- KIRKINIS, E. & OLVERA DE LA CRUZ, M. 2023 Taylor columns and inertial waves in a three-dimensional odd viscous liquid. *arXiv:2306.15536*.
- KIRKINIS, E., MASON, J. & OLVERA DE LA CRUZ, M. 2022 Odd viscosity-induced passivation of Moffatt vortices. *Journal of Fluid Mechanics* **950**, A19.
- KUZNETSOV, E.A. & DIAS, F. 2011 Bifurcations of solitons and their stability. *Physics Reports* **507** (2-3), 43–105.
- LANDAU, L. D. & LIFSHITZ, E. M. 1960 *Electrodynamics of Continuous Media*. Oxford: Pergamon Press.
- LANDAU, L. D. & LIFSHITZ, E. M. 1980 *Course of theoretical physics. Vol. 5: Statistical physics*. Oxford: Pergamon Press.
- LANDAU, L. D. & LIFSHITZ, E. M. 1987 *Fluid Mechanics. Course of Theoretical Physics, Vol. 6*. Pergamon Press Ltd., London-Paris.
- LAPA, M.F. & HUGHES, T.L. 2014 Swimming at low Reynolds number in fluids with odd, or Hall, viscosity. *Physical Review E* **89** (4), 043019.
- LIFSHITZ, E. M. & PITAEVSKII, L. P. 1981 *Course of theoretical physics. Vol. 10: Physical Kinetics*. Pergamon Press.
- LIGHTHILL, J. 1978 *Waves in Fluids*. Cambridge University Press.
- LOPEZ, J.M. & MARQUES, F. 2016 Inertial waves in rapidly rotating flows: a dynamical systems perspective. *Physica Scripta* **91** (12), 124001.
- LOWMAN, N.K. & HOEFER, M.A. 2013 Dispersive shock waves in viscously deformable media. *Journal of Fluid Mechanics* **718**, 524–557.
- MAAS, L.R.M. 2001 Wave focusing and ensuing mean flow due to symmetry breaking in rotating fluids. *Journal of Fluid Mechanics* **437**, 13–28.
- MANDERS, A.M.M. & MAAS, L.R.M. 2003 Observations of inertial waves in a rectangular basin with one sloping boundary. *Journal of Fluid Mechanics* **493**, 59–88.
- MARKOVICH, T. & LUBENSKY, T.C. 2021 Odd viscosity in active matter: microscopic origin and 3d effects. *Physical Review Letters* **127** (4), 048001.
- MOFFATT, H.K. 1964 Viscous and resistive eddies near a sharp corner. *J. Fluid Mech* **18** (1), 1–18.
- NOSAN, Ž., BURMANN, F., DAVIDSON, P.A. & NOIR, J. 2021 Evanescent inertial waves. *Journal of Fluid Mechanics* **918**, R2.
- OSTROVSKY, L.A. & POTAPOV, A.I. 1999 *Modulated Waves*. The Johns Hopkins University Press.
- PELZ, R.B., YAKHOT, V., ORSZAG, S.A., SHTILMAN, L. & LEVICH, E. 1985 Velocity-vorticity patterns in turbulent flow. *Physical Review Letters* **54** (23), 2505.

- SONI, V., BILIGN, E.S., MAGKIRIADOU, S., SACANNA, S., BAROLO, D., SHELLEY, M.J. & IRVINE, W.T.M. 2019 The odd free surface flows of a colloidal chiral fluid. *Nature Physics* **15** (11), 1188–1194.
- SOUSLOV, A., DASBISWAS, K., FRUCHART, M., VAIKUNTANATHAN, S. & VITELLI, V. 2019 Topological waves in fluids with odd viscosity. *Physical Review Letters* **122** (12), 128001.
- SPRENGER, P. & HOEFER, M.A. 2017 Shock waves in dispersive hydrodynamics with nonconvex dispersion. *SIAM Journal on Applied Mathematics* **77** (1), 26–50.
- WHITEHEAD, J.P. & WINGATE, B.A. 2014 The influence of fast waves and fluctuations on the evolution of the dynamics on the slow manifold. *Journal of Fluid Mechanics* **757**, 155–178.

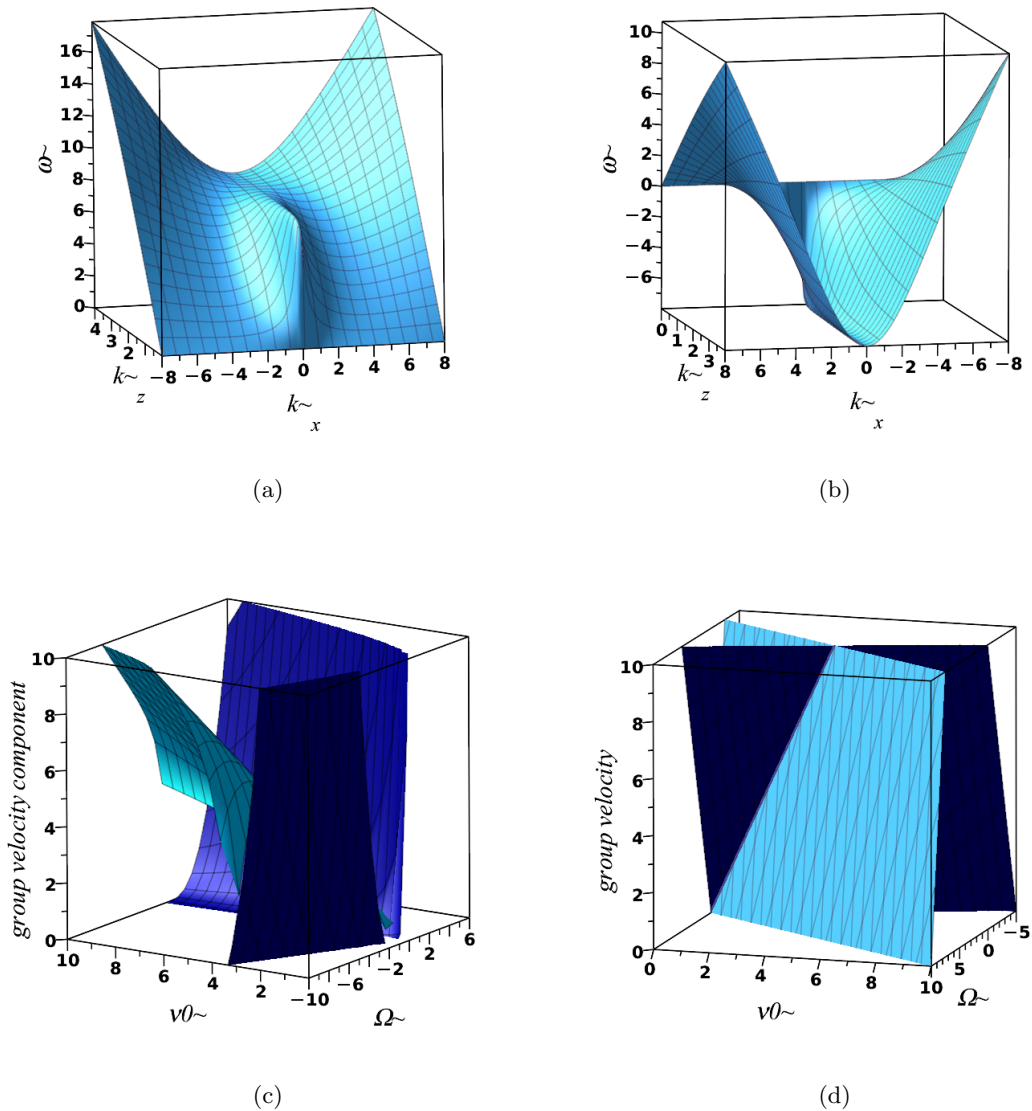


Figure 18: (a) and (b): Plane-polarized wave dispersion  $\omega$  (Eq. (5.4)) versus the wavenumbers  $k_x$  and  $k_z$  for  $\nu_o = 0.5$ ,  $\Omega = 4$  (a) and  $\Omega = -4$  (b). It is clear that both dispersion surfaces develop a saddle leading to the vanishing of the second derivative  $|\partial_{k_i k_j}^2 \omega|$ , implying the presence of caustics and a breakdown of the longtime asymptotics. (c): Group velocity components evaluated at a zero of  $|\partial_{k_i k_j}^2 \omega|$  displayed in the second line of Table 2 (light and dark color denotes  $x$ - and  $z$ - components respectively). (d) The  $z$ -component of group velocity in the first (light color) and third (dark color) lines of Table 2.

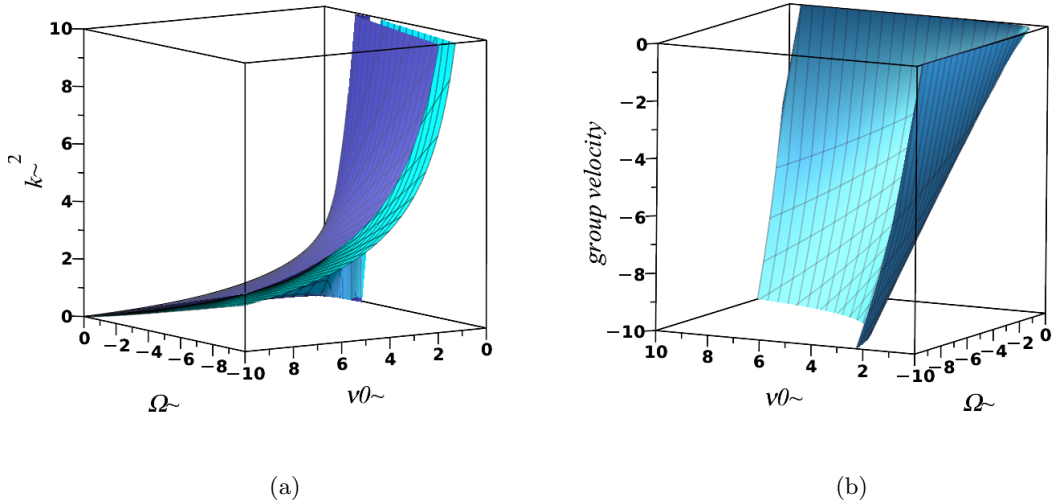


Figure 19: (a) Roots  $k^2$  from Eq. (7.9) of the determinant of the second derivative of the dispersion in (7.8) exist only for specific values of the parameters. Here we've set  $c = 1$ . Dark and light surfaces correspond to the first and second roots in (7.9) respectively. (b): Group velocity components evaluated at the second zero of  $|\partial_{k_i k_j}^2 \omega|$  (the light surface in the first panel of the figure)

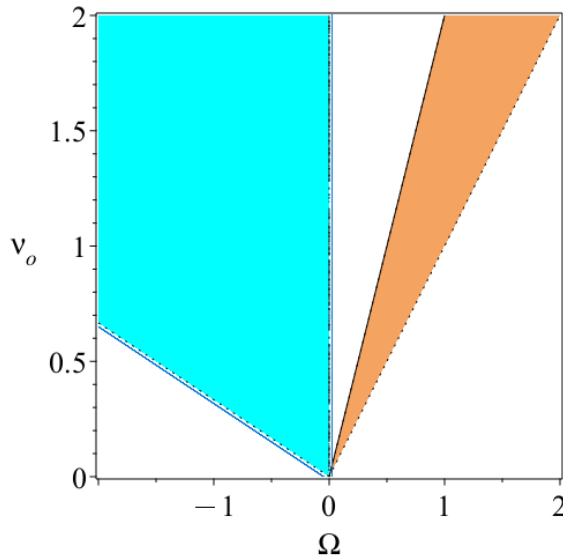


Figure 20: Allowed parameter values for the existence of roots of the second derivative of  $\omega$  in (5.12) as they appear in Table 2. The cyan colored area corresponds to the region in parameter space ( $F < 5\nu_o k^2$ ) for the root appearing in the second line of Table 2. The sand-brown colored area is the region in parameter space ( $0 < 2\Omega - \nu_o k^2 < \nu_o k^2$ ) for the roots in the first line of Table 2.